Biomaterials 276 (2021) 121049

Contents lists available at ScienceDirect

Biomaterials

journal homepage: www.elsevier.com/locate/biomaterials

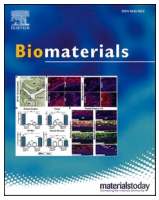

Repopulation of decellularized retinas with hiPSC-derived retinal pigment epithelial and ocular progenitor cells shows cell engraftment, organization and differentiation

Maria Maqueda [a,1], Jose Luis Mosquera [a,1], José García-Arumí [b], Anna Veiga [c,d], Anna Duarri [b,d,*]

[a] Bioinformatics Unit, Institut d'Investigació Biomèdica de Bellvitge – IDIBELL, L'Hospitalet de Llobregat, Barcelona, Spain
[b] Ophthalmology Research Group, Vall d'Hebron Institut de Recerca - VHIR, Vall d'Hebron Hospital Universitari, Barcelona, Spain
[c] Pluripotent Stem Cell Therapy Group, Regenerative Medicine Program, Institut d'Investigació Biomèdica de Bellvitge – IDIBELL, L'Hospitalet de Llobregat, Barcelona, Spain
[d] National Stem Cell Bank-Barcelona Node, Biomolecular and Bioinformatics Resources Platform (PRB2), ISCIII, Madrid, Spain

ARTICLE INFO

Keywords:
Tissue engineering
Decellularization
Recellularization
Extracellular matrix
ECM
Retina
RPE
Scaffolds
Ocular progenitors

ABSTRACT

The retinal extracellular matrix (ECM) provides architectural support, adhesion and signal guidance that controls retinal development. Decellularization of the ECM affords great potential to tissue engineering; however, how structural retinal ECM affects *in vitro* development, differentiation and maturation of ocular cells remains to be elucidated. Here, mouse and porcine retinas were decellularized and the protein profile analyzed. Acellular retinal ECM (arECM) scaffolds were then repopulated with human iPSC-derived retinal pigment epithelial (RPE) cells or ocular progenitor cells (OPC) to assess their integration, proliferation and organization. 3837 and 2612 unique proteins were identified in mouse and porcine arECM, respectively, of which 93 and 116 proteins belong to the matrisome. GO analysis shows that matrisome-related proteins were associated with the extracellular region and cell junction and KEGG pathways related to signalling transduction, nervous and endocrine systems and cell junctions were enriched. Interestingly, mouse and porcine arECMs were successfully repopulated with both RPE and OPC, the latter exhibiting cell lineage-specific clusters. Retinal cells organized into different layers containing well-defined areas with pigmented cells, photoreceptors, Müller glia, astrocytes, and ganglion cells, whereas in other areas, conjunctival/limbal, corneal and lens cells re-arranged in cell-specific self-organized areas. In conclusion, our results demonstrated that decellularization of both mouse and porcine retinas retains common native ECM components that upon cell repopulation could guide similar ocular cell adhesion, migration and organization.

1. Introduction

The eye is a complex organ formed by specialized tissues developed from different cell lineages. Located in the posterior pole of the eye, the retina is the functional part that converts light stimulus into electric signal to be processed in the brain. During retinal development, multipotent retinal progenitor cells, which are developed from the neuroectoderm, give rise to all types of neurons and the Müller glia in a sequential manner [1,2]. The specification of retinal cell fate is controlled by (i) intrinsic factors such as transcription factors and miRNAs [3]; (ii) extrinsic factors including retinal extracellular matrix (ECM) composition [4]; iii) dynamics of retinal progenitors [5]; and/or iv) stochastic mechanisms. The retinal ECM provides architectural support, adhesion and signal guidance that controls cell survival, proliferation, maturation, organization and polarity to shape this ocular tissue. Retinal ECM has its own compositions and changes during retinal development [6] and, in each stage of retinogenesis, the ECM influences cellular organization, differentiation and axonal development via specific signals [6,7]. In addition to retinal ECM, the retinal pigment epithelium (RPE) also produces and secretes ECM proteins and factors and, together with Bruch's membrane, modulate the maturation of retinal development [8,9], and maintain retinal integrity and functions

* Corresponding author. Vall d'Hebron Research Institute, Vall d'Hebron Barcelona Hospital Campus, Passeig Vall d'Hebron 119-129, 08035, Barcelona, Spain.
E-mail address: anna.duarri@vhir.org (A. Duarri).
[1] These authors contributed equally to this work.

https://doi.org/10.1016/j.biomaterials.2021.121049
Received 13 February 2021; Received in revised form 22 July 2021; Accepted 23 July 2021
Available online 24 July 2021

[10–12]. Overall, the posterior ocular ECM plays a key role in retinal cell differentiation as well as in tissue repair and regeneration.

The ECM consists of a complex protein network derived from basement membranes, vasculature and interstitial matrix called matrisome [13,14]. The matrisome comprises the core matrisome and the ECM-associated proteins. The former is composed of extracellular matrix proteins, such as collagens, proteoglycans and glycoproteins. The latter includes secreted factors and regulators that are bound to the ECM and represent the source of modulating signals, such as fibroblast growth factor family, taurine or retinoic acid, involved in retinogenesis, Naturally derived ECM from tissues and organs has been used for multiple purposes, from complex tissues and organ regeneration to simple replacement treatments to create synthetic scaffolds and matrices. It has been reported and used in a number of applications involving various tissues and organs such as cornea, kidney, heart, lungs, liver, valve, trachea, retina and blood vessels as reviewed in Ref. [15]. The process to obtain these biological scaffolds is decellularization, which aims to deprive the ECM of native cells and DNA material while maintaining its mechanical, biological and structural properties. Decellularization offers great potential to the tissue engineering field and is particularly interesting for engineering ocular tissue. Currently, some studies aimed to assess the use of acellular ECM derived from retina, choroid and Bruch's membranes as scaffolds to culture different retinal cells [16–21]. The generation of films from decellularized bovine retinas has been used as supports to culture human retinal progenitor cells [18]. Similarly, the production of Bruch's membrane-like matrix from ARPE19 cells has been used to support RPE cell growth, favouring their maturation and pigmentation [19]. ARPE19 cells deposited some of the ECM proteins, such as fibronectin, laminin and collagen type I, but failed to produce elastin and collagen type IV. Despite that, RPE cells cultured on this ECM retained pigmentation and expressed more RPE65 compared with other substrates, indicating that acellular ECM may retain structural proteins and molecular cues that promote retinal maturation. More recently, Dorgau et al., used peptides from decellularized bovine neural retinas and RPE to generate retinal organoids with increased rod photoreceptor number and enhanced light responses [17]. Although there is evidence that the ECM film surface or peptides improved retinal progenitor and RPE cell maturation, the full characterization of complex 3D retinal ECM morphology and its recellularization capacity has not been addressed yet. Thus, the better understanding of how structural retinal ECM effects *in vitro* development, differentiation and maturation of ocular progenitor cells is particularly interesting.

To determine whether acellular retinas are suitable 3D ECM scaffolds for the correct maturation of ocular cells, we here decellularized mouse and porcine retinas and we obtained their protein profile. Then, these acellular retinal ECMs were subsequently repopulated with human induced pluripotent stem cell-derived RPE cells or multi-zone ocular progenitor cells to emulate the natural complexity of the eye. This work aims to establish a better microenvironmental niche for ocular cell development *in vitro* and to deepen the understanding of the extrinsic cues and cell fate determinants present in the acellular retinal ECM that regulate differentiation and modulate cell fate decisions and organization.

2. Methods

2.1. Isolation and decellularization of retinas from murine and porcine eyes

All procedures were approved by the Animal Care and Use Committee of the IDIBELL and were performed in accordance with the tenets of the European Community (86/609/CEE), the Association for Research in Vision and Ophthalmology and NIH Publications No. 8023, revised 1978.

Murine eyes (~200) were collected from 1 to 2 month-old CD-1 albino mice. Mice were euthanized and eyes were enucleated and kept on phosphate saline buffer (PBS) containing penicillin and streptomycin (P/S). The porcine eyes (6 eyes) were collected fresh from adult domestic pigs from the abattoir within 1 h of death. Dissection of retinas was performed under the loupe in phosphate saline buffer (PBS) containing penicillin/streptomycin (P/S) by removing the cornea, the lens and vitreous humour, and eye-cups were peeled to remove retinas from RPE. A few native retinas were processed for further characterization.

Retinas were decellularized at room temperature (RT) in agitation (50 rpm) using a step-wise protocol. After retinal dissection, mouse and porcine retinas were first treated with distilled water in the presence of Turbo DNase I (Abmion) (2 h) to prevent agglutination of DNA and to reduce fragment length. Then, retinas were treated with two different surfactants: non-ionic detergent, 0.5 % Triton X-100 in distilled water (overnight), less harsh to the tissue; and ionic-detergent, 0.1 % sodium dodecyl sulphate (SDS) in distilled water (2 h) to solubilized cell membranes, followed by extensive washes with distilled water (2 × 30 min) followed by PBS supplemented with P/S (24 h) (Fig. 1A). Decellularized retinal ECMs were kept in PBS supplemented with P/S at 4 °C for further use.

2.2. DNA quantification

Native and acellular retinas were wet weighed and treated with Proteinase K (0.1 mg/ml) in 10 mM Tris pH 8 (50 mM NaCl, 1 mM EDTA) at 50 °C O/N. DNA extraction was performed with the QIAamp DNA mini kit (Qiagen) following manufacturer's specification and eluted with 50 μl distilled water. DNA content was measured in a Nanodrop spectrophotometer. Residual DNA was normalized to the corresponding wet weight.

2.3. Electron microscopy

For scanning electron microscopy (SEM), native and decellularized retinas were fixed with 2.5 % (w/v) glutaraldehyde in 0.1 M cacodylate buffer pH 7.2–7.4 for 2 h at 4 °C. Fixed tissue underwent serial dehydration in ascending ethanol series, followed by treatment with the critical point dryer or alternatively, with hexamethyldisilazane to replace critical point drying in the preparation of mouse acellular retina to preserve its structure. Then, retinas were metalized and examined under a JEOL JSM-6390LV scanning electron microscope (JEOL, Tokyo, Japan).

2.4. Liquid chromatography-tandem mass spectrometry (LC-MS/MS)-based proteomic study

Two biological replicates of pig acellular retinas and two pools of 5 technical replicates of mouse acellular retinas were analyzed by LC-MS/MS to obtain the complete proteome. The proteins were extracted with 1 % SDS, 100 mM DTT, 100 mM Tris-HCl pH 7.6, sonicated for 10 min in an ultrasound batch and finally boiled for 5 min at 95 °C. The samples were then centrifuged at 16,000 g for 5 min and the supernatants recovered in new tubes. The protein was quantified with the RCDC protein assay kit and 12 μg of each sample were digested with LysC/Trypsin by using a Filter-Aided Sample Preparation (FASP) protocol. Finally, the samples were analyzed by LC-MS/MS. The LC separation was conducted on an Easy-nLC 1000 (Thermo) using 0.1 % formic acid

as Solvent A and acetonitrile with 0.1 % formic acid as B. Each run was carried out at 250 nL/min with a gradient of 95 % of solvent A to 65 % A in 180 min. Blank samples with solvent A injections were run in between each sample. Sample was concentrated in an Acclaim PepMap 100 trap column (Thermo), and fractionated in a Nikkyo Technos Co., 75 μm ID, 3 A pore size, 12.5 cm in length with built in emitter column, coupled to a Nanospray Flex (Thermo) ESI source. Shotgun LC-MS/MS analysis was performed online with an electrospray voltage of 1.9 kV using a Q Exactive HF mass spectrometer (Thermo) with HCD fragmentation using top 15 precursor with charge 2 to 5 for data-dependent acquisition (DDA).

2.5. Data processing, database searching and protein annotation

Software (version 1.6.2.6a, www.maxquant.org) as described [22] supported by Andromeda was used as the database search engine for peptide identifications [23]. MS/MS peak lists were generated by filtering spectra to contain at most six peaks per 100 Th intervals and searched by Andromeda against a concatenated forward and reversed version of the Mus Musculus and Sus Scrofa Swiss-Prot databases, respectively. The databases were downloaded from UniProt (www.uniprot.org) on December 2018 [24] consisting of 17,001 and 1427 protein entries, respectively. Additionally, in the case of Sus Scrofa, the TrEMBL database was also considered, and downloaded on May 2019, due to the non-existent collagen-related proteins in the Swiss-Prot database for this organism. This unreviewed protein list included 332, 500 different accession entries. The searches were filtered using a False Discovery Rate (FDR) at the peptide and protein level set at 5 %.

2.6. Bioinformatics analysis

All data analysis was conducted in R version 3.6 (http://www.R-project.org/) using specific packages from Bioconductor version 3.9 [25].

2.7. Identification of matrisome-related proteins

Two final lists of retrieved proteins from mouse and porcine acellular retinas, referred to as total proteome, were available for the downstream analysis. Proteins were annotated with their corresponding accession number and gene name. Entrez Gene IDs were also mapped using the annotations from *org.Mm.eg.db* and *org.Ss.eg.db* packages, both version 3.8.2 [26,27]. Relevant human orthologs were retrieved from Ensembl release 95 using the *biomaRt* package version 2.40.5 [28–30].

To identify matrisome related proteins, the database provided by The Matrisome Project initiative was used [14]. This database collects those genes encoding the ECM, *aka* core matrisome, and ECM-associated proteins, *aka* matrisome-associated. Additionally, these categories are each divided into three subcategories: ECM-glycoproteins, collagens and proteoglycans for core matrisome and ECM-affiliated proteins, ECM-regulators and secreted factors for ECM-associated. The related murine and human data was downloaded from http://matrisomeproject.mit.edu in March 2019. In the case of *Mus musculus*, official gene symbols were used for match searches in the murine matrisome. For *Sus scrofa*, the annotated human gene orthologs were used in the human matrisome.

2.8. Gene Ontology distribution analysis

To analyze the Gene Ontology (GO) distribution, GO terms for each UniProt accession number were annotated [31]. The analysis was conducted separately over the total proteome lists and their relevant matrisome subsets. The three GO biological domains, Biological Process (BP), Molecular Function (MF) and Cellular Component (CC), were considered. For this purpose, all GO annotations were downloaded from the EMBL-EBI ftp site (ftp://ftp.ebi.ac.uk/pub/databases/GO/goa/) in April 2019 for the organisms of interest. Per annotated GO term, their ancestors were retrieved using the *GO.db* package version 3.8.2 [32]. One table per ontology and organism was built with the list of all mapped GO terms, including ancestors. This table was ranked by the number of annotated proteins in each mapped term.

To localize proteins to the main cellular compartments (extracellular, plasma membrane and intracellular), the following GO CC terms were used: GO:0005615 ('Extracellular space') and GO:0005576 ('Extracellular region') for extracellular location, GO:0043226 ('Organelle') and GO:0005829 ('Cytosol') for intracellular location and GO:0005886 ('Plasma membrane') for plasma membrane.

To summarize the GO distribution, a set of GO terms were selected as representative of a particular ontology. For the BP domain, all GO:0008150 ('Biological Process') children terms were considered obtaining 32 GO BP terms. For the MF domain, all GO:0003674 ('Molecular Function') children terms were considered obtaining 15 GO BP terms. For the CC domain, nine terms were manually selected as GO:0005575 ('Cellular Component') children terms was too general. Specifically, GO:0005576 ('Extracellular region'), GO:0005634 ('Nucleus'), GO:0005829 ('Cytosol'), GO:0005739 ('Mitochondrion'), GO:0005783 ('Endoplasmic Reticulum'), GO:0005794 ('Golgi Apparatus'), GO:0005886 ('Plasma Membrane'), GO:0005856 ('Cytoskeleton') and GO:0097458 ('Neuron Part'). For every selected GO term, the number of annotated proteins to that specific term was used to compute the GO distribution. Bar plots were generated, one per domain and organism, with the percentages obtained. Total proteome and matrisome-related protein distributions were jointly represented by means of the *ggplot2* package version 3.1.1 allowing a visual comparison [33].

2.9. Functional analysis

To put the different sets of genes obtained from the total proteome or matrisome-related proteins into biological context, a gene enrichment analysis (GEA) was applied to the corresponding lists of Entrez Gene IDs. GEA was computed over the Kyoto Encyclopedia of Genes and Genomes (KEGG) PATHWAY [34] and GO databases. For this purpose, the *clusterProfiler* package version 3.12.0 was used [35]. For each queried biological pathway or GO term, a p-value was calculated using a hypergeometric distribution test. Benjamini-Hochberg correction was applied for multiple testing [36]. A False Discovery Rate (FDR) < 1 % was considered as statistically significant. The background distribution was defined by all available annotations in the relevant database. Category and subcategory were annotated to every overrepresented KEGG pathway according to the database map. In order to reduce the Redundancy of enriched GO terms, the initial list of overrepresented terms was simplified based on their semantic similarity. Additionally, every overrepresented GO term was related to the main node (BP, MF or CC) children and grandchildren terms according to the database hierarchy.

2.10. Human induced pluripotent stem cell culture

The human induced pluripotent stem cell (hiPSC) line FiPS-4F-7 was obtained from the Spanish National Stem Cell Bank after approval by the Ethics Review Board and the Catalan Authority. hiPSC were cultured and expanded in Matrigel (Corning) pre-coated plates with mTeSR1 medium (StemCell Technologies) at 37 °C and 5 % CO_2. Cell lines were passaged with 1 mM EDTA in a 1:3–1:6 ratio every 5–7 days and characterized as described [37].

2.11. Differentiation of hiPSC into ocular progenitor cells and retinal pigment epithelium cells

The differentiation protocol to obtain multi-zone ocular progenitor cells (OPCs) from hiPSC in 2-dimensions was that previously described with some modifications [38]. The eye-field commitment was induced from 60 % confluent hiPSC cultures on Matrigel by the induction medium (IM), consisting of Dulbecco's Modified Eagle's Medium/Nutrient Mixture F-12 (DMEM/F12), 5 % Foetal Bovine Serum, 0.1 mM non-essential amino acids, 2 mM GlutaMax, 1 % N2, 1 % B27, 10 mM β-glycerolphosphate, and 10 mM nicotinamide, supplemented with recombinant human IGF-1 (10 ng/ml), Noggin (10 ng/ml), DKK-1 (10 ng/m), bFGF (5 ng/ml) until day 30. At this point, OPCs comprised neuroectoderm (retinal progenitor cells and retinal pigment epithelial cells), surface ectoderm (corneal, conjunctiva, limbal and lens progenitor cells), and stromal cells (Suppl. Figure S9).

Differentiation of hiPSC towards retinal pigment epithelial (RPE) cells and transduction with lentiviral particles carrying GFP gene reporter were previously described [39,40].

2.12. Recellularization of acellular retinal ECM

Mouse and porcine acellular retinas (arECM) were equilibrated in DMEM/F12 in the presence of P/S for 30 min at 37 °C and 5 % CO_2 prior to the recellularization process. RPE-GFP cells at passage 4–5, or OPC at day 30 of differentiation, were disaggregated in TrypLE select to obtain a single cell suspension. RPE cells were resuspended IM medium supplemented with IGF-1 (10 ng/ml), and OPC were resuspended in IM medium supplemented with IGF-1 (10 ng/ml) and all-trans retinoic acid (500 nM). RPE or OPC single cell suspensions (5×10^4 cells) were added to each mouse or porcine arECM in single wells of a low-attachment, round bottom, 96 well-plate in a total volume of 50 μl and cultured at 37 °C and 5 % CO_2 (n = 3 biological replicates and >5 technical replicates each). At day 1, 50 μl of fresh medium was added to each well and at day 2, medium containing non-attached cells was removed from the wells and replaced with fresh medium. Medium was changed every other day for up to 110 days culture.

2.13. Histology and immunochemistry

Native, decellularized and recellularized retinas and cells were fixed in 4 % paraformaldehyde (PFA) overnight at 4 °C and washed in PBS. Native and recellularized retinas were embedded in paraffin and a 3 μm section obtained. Conventional haematoxylin and eosin staining of tissue sections was performed by standard protocols and images acquired with a FSX100 microscope (Olympus Life Science).

For immunohistochemistry (IHC), paraffin sections were deparaffined and antigens were retrieved with citrate buffer pH = 6 at 100 °C. Then, retinas, paraffin sections and cells were permeabilized and blocked in PBS, 0.5 % Triton-X100, 6 % Donkey serum during 1 h at RT. Primary antibodies were diluted in PBS, 0.1 % Triton-X100, 6 % Donkey serum overnight at 4 °C and secondary antibodies were incubated for 2 h at 37 °C in the same buffer. Primary antibodies are listed in Suppl. Table S1. Nuclei were stained with 4′,6-diamidino-2-phenylindole (DAPI). Confocal images were taken with a DM6000 (Leica) and processed using ImageJ and Photoshop.

2.14. Real time-quantitative PCR

Total messenger RNA was isolated from cells using the PureLink RNA Mini Kit (Invitrogen). 1 μg of mRNA was reverse transcribed with the High-Capacity cDNA Reverse-Transcription Kit (Applied Biosytems) and SYBR green (Invitrogen) was used in a standard reaction [41]. Standard PCR reactions were performed using the MyTaq Red DNA Polymerase (Bioline GmbH) and DNA was visualized in 2 % agarose gels. For real-time quantitative PCR reactions, SYBR green (Invitrogen) was used in a standard reaction. Cycle threshold (Ct) values were normalized using *GAPDH* as a housekeeping gene. Assays were run on the ABI PRISM 7900HT platform (Applied Biosystems) and data analyzed using the $2^{-\Delta Ct}$ method. Data represents at least 3 different experiments and are presented as mean ± standard deviation. Statistical analysis was performed using GraphPad Prism software (GraphPad Software Inc.) and tested with Student's *t*-test; p values < 0.01. The primers used are listed in Suppl. Table S2.

2.15. In vitro photoreceptor outer segment phagocytosis assay

Phagocytosis activity of RPE-repopulated mouse arECM and RPE cell culture was assessed by analyzing the binding and internalization of photoreceptor outer segments (POS) labelled with fluorescein isothiocyanate (FITC), as described previously [40]. Labelled isolated bovine POS were obtained from Fondation Voir et Entendre (Paris, France) [42]. FITC-POS were resuspended in DMEM/F12, added to RPE-repopulated mouse arECM and RPE cells and incubated for 12 h at 37 °C with 5 % (v/v) CO2. Then, RPE-repopulated ECM and cells washed four times in PBS with Ca2+ and Mg2+ and fixed in 4 % (w/v) paraformaldehyde for 20 min at room temperature. Immunostaining was performed as described above. Confocal images were taken with a TCS SP5 confocal microscopy (Leica Microsystems). For quantitative calculation, 3 random fields of view (382 μm × 382 μm) were photographed per group and the number of internalized POS was counted. Three independent experiments were conducted.

3. Results

3.1. Decellularization of mouse and porcine retinas

Native retina possesses different membranes and matrices, such as basement membranes, interphotoreceptor matrix, outer and inner plexiform layers, and retinal vasculature composed of laminins, collagens and other ECM proteins (Suppl Figure S1A) [42]. The decellularization process aims to remove all cells and genetic material from retinas to obtain acellular retinal ECM (arECM). In order to examine whether the decellularization process preserves ECM structure and protein content, isolated mouse and porcine retinas were treated following a protocol based on a hypoosmotic shock followed by two different detergents, Triton X-100 and SDS. During the process of decellularization, retinas become translucent, preserving their native structures (Fig. 1A-A′). The ultrastructure of acellular retinas revealed that the cellular content was lost in comparison with native retinas, while the vasculature, matrix proteins and basement membranes remained (Fig. 1B-B′). Note that due to the softness of retinas, the whole structure was difficult to maintain intact in SEM analysis. Moreover, via immunohistochemistry (IHC), we found that both mouse and porcine arECMs retained typical ECM proteins such as collagens I and IV, fibronectin, laminin and chondroitin sulphate (a glycosaminoglycan or GAG) (Fig. 1C-C'; Suppl Figure S1B). In line, after cell removal, the DNA content in arECM was reduced to 6 % compared with native retinas (Fig. 1D).

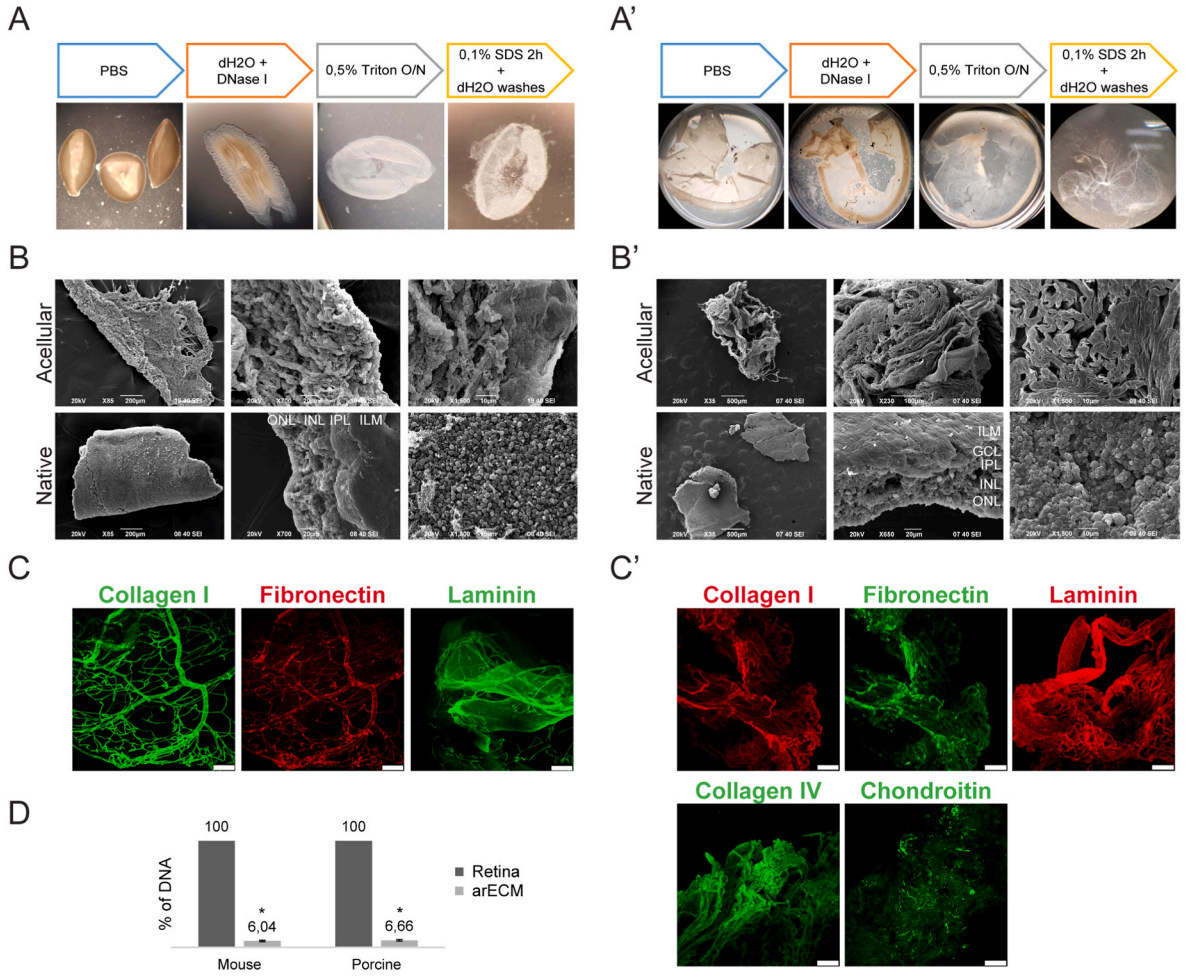

Fig. 1. Decellularization of mouse and porcine retinas. A-A′). Schematic representation of the decellularization process of CD-1 mouse eyes (A–C) and domestic porcine eyes (A′-C′) consisting in distilled water with DNase I for 1 h, 0.5 % Triton X-100 overnight (O/N) and 0.1 % SDS for 1 h followed by extensive rising with distilled water followed by PBS washes. Images show the macroscopic appearance of retinas becoming more translucent during each decellularization steps. B–B′) Scanning electron microscopy (SEM) images of acellular mouse (B) and porcine (B′) retinas (top panels) compared with native retinas (bottom panels) show preservation of retinal membranes and vascular structures. GCL, ganglion cell layer; ILM, inner limiting membrane; INL, inner nuclear layer; IPL, inner plexiform layer ONL, outer nuclear layer. C–C′) Immunofluorescent images of whole-mount acellular retinal ECM containing ECM proteins collagens I and IV, fibronectin, laminin and chondroitin sulphate. Scale bar: 100 μm. D) Quantification of DNA remaining in the mouse and porcine arECM compared with their native retinas. Data are expressed as mean ± SD (three independent biological replicates), *p < 0,001 calculated using Student's *t*-test.

3.2. Proteomic analysis indicated a preservation of the ECM proteome in the decellularized retinas

3.2.1. Core matrisome - ECM glycoproteins was the most abundant subcategory

We profiled the total protein composition of mouse and porcine arECM proteomes by mass spectrometry. A total of 26,044 peptides were identified in mouse arECM and 1097 peptides in porcine arECM (Suppl. Excel 1 and Suppl. Excel 2). The final lists of total proteomes included 3837 and 2612 unique proteins, encoded by 3833 and 928 unique genes in *Mus musculus* and *Sus scrofa*, respectively. For *Sus scrofa*, 91.9 % of the proteins were retrieved from the TrEMBL database since we observed that no type of collagen protein was present in the Swiss-Prot database.

Among all the genes, 93 (mouse) and 116 (porcine) different genes were related to the matrisome, which is divided into core matrisome and matrisome-related proteins (Fig. 2A; Suppl. Table S3). In both organisms, most of these genes (60–65 %) belonged to the core matrisome category, where ECM glycoproteins were the most abundant subcategory with a representation of 40.9 % (mouse) and 44.8 % (porcine) (Fig. 2A; Suppl. Excel 1 and Suppl. Excel 2). The remaining genes were distributed similarly among the other subcategories. No significant differences were found between mouse and porcine matrisome distribution (Fisher's exact test, p-value > 0.05). Some of the most abundant core matrisome proteins detected were collagen types I and II (collagens); laminin and agrin (glycoproteins); and heparan sulphate and biglycan (proteoglycans) (Table 1). Among the ECM-associated proteins, we found regulators such as serphin H1, LOXL2/3 and transglutaminase 2; ECM-affiliated proteins annexins, plexins and chondroitin sulphate; and secreted factors such as calcium-binding proteins S100A11, FGF2 and multiple epidermal growth factor 6 (Table 1), common proteins found in other acellular ECMs from different tissues [43].

3.3. Gene Ontology (GO) distribution in total proteome and matrisome-related proteins

The occurrence of every GO term was collected for *Mus musculus* (Suppl. Excel 1) and *Sus scrofa* (Suppl. Excel 2) organisms. Most of the proteins (>97 %) in mouse arECM total proteome and matrisome-related subset were annotated, at least, to one GO term, independently of the ontology domain (Suppl. Table S4). However, only 32 % of porcine arECM total proteome were present at least in one GO term annotation. This was because porcine proteins retrieved from the

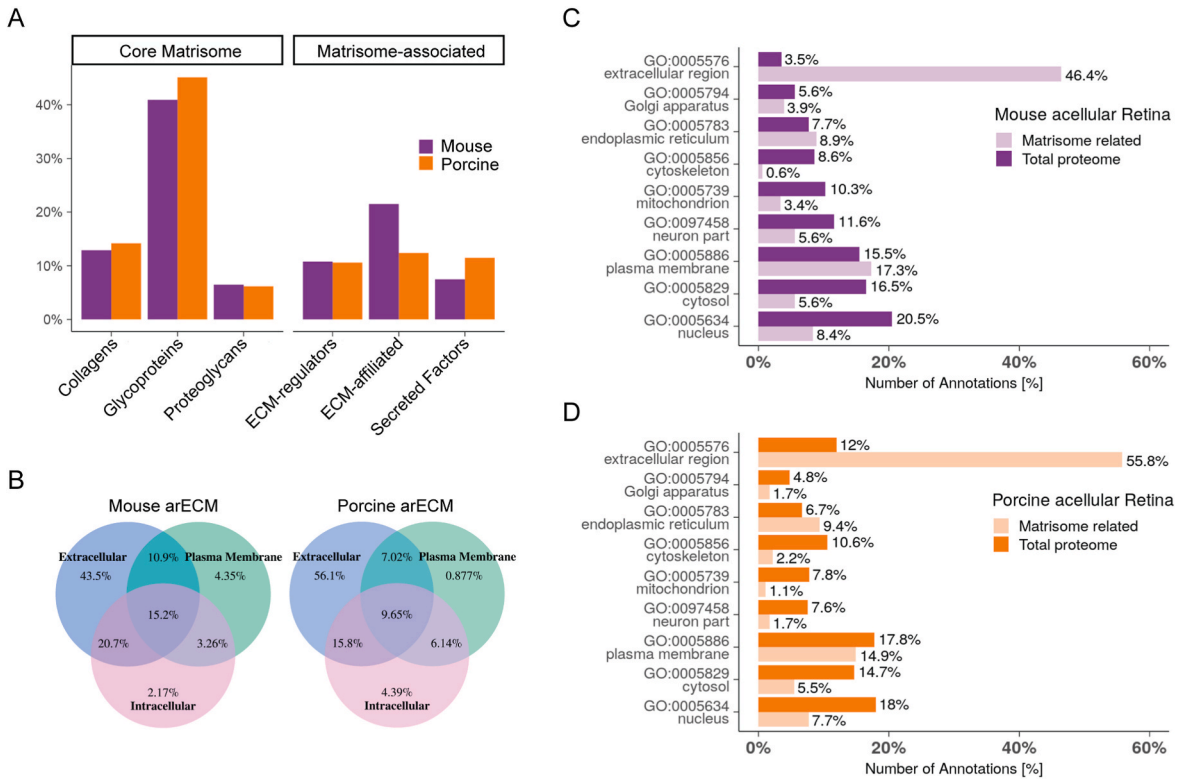

Fig. 2. Proteomic analysis of mouse and porcine acellular retinal ECM. A) Percent distribution of matrisome-related genes for mouse and porcine decellularized retinas. Core matrisome and matrisome-associated main categories and respective subcategories from 'The Matrisome Project' were considered [13]. Percentages were computed considering the 93 out of the 3833 unique genes from mouse arECM and 116 out of the 928 unique genes from porcine arECM. B) Venn diagrams show the subcellular localization (extracellular, intracellular and plasma membrane) distributions of the set of proteins included in the matrisome-related subset for matrisome-related proteins of mouse (left, 93 unique proteins) and porcine (right, 265 unique proteins) arECM. C) and D) Distribution of Gene Ontology (GO) Cellular Component (CC) terms distribution annotations for total proteome and matrisome-related proteins of mouse and porcine arECM, respectively. Nine main CC terms under GO:0005575 ('Cellular Component') hierarchy are considered. Percentages referred to all protein annotations retrieved from these nine terms, specifically, for (C) 7601 and 179 annotations and for (D) 1354 and 181 in the case of total proteome and matrisome respectively. GO terms are sorted based on the *Mus musculus* total proteome percentage.

TrEMBL database represented 99 % of these proteins with no annotation. In the matrisome-related protein subsets of both organisms, there were proteins simultaneously annotated to GO CC terms in extracellular, plasma membrane and intracellular regions, although proteins exclusively located in the extracellular region were more represented with 43.5 % and 56.1 % of mouse and porcine arECM, respectively (Fig. 2B). More than 93 % of the GO terms mapped to the total proteome proteins were shared by both organisms (Suppl. Table S5). For the CC domain, the 'extracellular region' term of the matrisome-related proteins stood out (46.4 % and 55.8 % occurrence) from the rest of terms and from the total proteome (Fig. 2C and D). The distribution of GO BP is shown in Suppl. Figure S3 (mouse) and Suppl. Figure S4 (porcine) and GO MF domains in Suppl. Figure S5. Of note, in the case of BP ontology, the 'cellular process' term was the most annotated whereas "adhesion" was enriched in matrisome related proteins compared with total proteome. For the MF domain, 'binding' was the most represented term with percentages ranging from 45.8 % in mouse and 53.7 % in porcine matrisomes. These analyses suggest that arECM retained a high proportion of matrisome-related proteins involved in adhesion, proliferation and developmental processes.

3.4. Distribution differences between mouse arECM and native retinal matrisomes

We then compared our total proteome from mouse acellular retinas with the proteome of mouse native retinas provided by Harman et al., [44] that included 5288 unique proteins, of which 105 proteins were annotated in the matrisome category. We identified 79 % of our proteome to be common to both datasets, and 57 shared proteins belonged to the matrisome category (Suppl. Fig. S2). Protein distributions within matrisome categories showed statistically significant differences (Fisher's exact test, p-value < 0.05). Our acellular retinas were enriched in glycoproteins and collagens compared with native retinas, whereas the decellularization process decreased the presence of ECM regulators and secreted factors. Despite these differences, these results indicate that the decellularization protocol used in this study preserved the retinal ECM protein composition.

3.5. Mouse and porcine arECM proteomes overlap with the Human EyeOme catalogue

Moreover, the latest Human EyeOme catalogue included 9782 nonredundant proteins, corresponding to 9546 unique human genes, distributed in 11 different ocular tissues [45]. Based on relevant human orthologs of mouse (3,696) and pig (670), we found that 88.2 % and 94.5 % of our mouse and porcine proteomes, respectively, were represented in EyeOme. A total of 20.2 % and 9.7 % of these proteins found were exclusively expressed in the posterior segment of the eye, mostly identified in the retina, vitreous and the choroid/RPE (Fig. 3A–B; Suppl Excel 3). However, we detected that 77.4 % and 89 % of both proteomes were common in the anterior and posterior segments of the eyes, only 2.4 % and 1.3 % being exclusively from the anterior segment (Fig. 3; Suppl Excel 3). This data indicates that the tissue specificity of arECMs proteins is not restricted to only one tissue, but that arECM is composed of common ocular ECM proteins.

Table 1
Acellular retinal ECM protein profile. The list shows the most abundant proteins identified in mouse and porcine arECM for the core matrisome and the matrisome-related proteins.

	MOUSE		PIG	
	Gene symbol	Protein	Gene symbol	Protein
CORE MATRISOME PROTEINS				
COLLAGENS	Col4a2	Collagen alpha-2(IV) chain; Canstatin	COL12A1	Collagen alpha-1(XII)
	Col18a1	Collagen alpha-1(XVIII) chain; Endostatin	COL6A3	Collagen alpha-3(VI)
	Col4a1	Collagen alpha-1(IV) chain; Arresten	COL14A1	Collagen alpha-1(XIV)
			COL7A1	Collagen alpha-1(VII)
			COL18A1	Collagen alpha-1(XVIII)
GLYCOPROTEINS	Lama5	Laminin subunit alpha-5	*LAMA5*	Laminin subunit alpha-5
	Lamb2	Laminin subunit beta-2	LAMB2	Laminin subunit beta-2
	Lama2	Laminin subunit alpha-2	LAMC1	Laminin subunit gamma-1
	Lamc1	Laminin subunit gamma-1	FBN1	Fibrillin-1
	Agrn	Agrin	AGRN	Agrin
PROTEOGLYCANS	Hspg2	Basement membrane-specific heparan sulphate proteoglycan core protein; Endorepellin	HSPG2	Basement membrane-specific heparan sulphate proteoglycan core protein; Endorepellin
			BGN	Bigglycan
			PRELP	Prolargin
MATRISOME ASSOCIATED PROTEINS				
REGULATORS	Tgm2	Protein-glutamine gamma-glutamyltransferase 2	ITIH5	Inter-alpha-trypsin inhibitor heavy chain H5
	Serpinh1	Serpin H1	TGM2	Transglutaminase 2
	A2m	Alpha-2-macroglobulin	LOXL3	Lysyl oxidase homolog 3
			LOXL2	Lysyl oxidase homolog 2
ECM-AFFILIATED	Plxnb2	Plexin-B2	ANXA6	Annexin A6
	Anxa6	Annexin A6	ANXA2	Annexin A2
	Plxna1	Plexin-A1	ANXA1	Annexin A1
	Lman1	Protein ERGIC-53	ANXA5	Annexin A5
	Cspg4	Chondroitin sulphate proteoglycan 4		
SECRETED FACTORS	Hcfc1	Host cell factor 1	MEGF6	Multiple epidermal growth factor-like domains protein 6
	S100a11	Protein S100-A11	SFRP2	Secreted frizzled-related protein 2
	Megf6	Multiple epidermal growth factor-like domains protein 6	FGF2	Fibroblast growth factor
			CHRDL1	Chordin-like protein 1

The most abundant proteins (represented maximum of 5) based on the number of peptides (included in both replicates) within fourth quartile that represents the 25 % most abundant peptides in each category.

3.6. Functional analysis results highlighted synapse junction related GO terms and nervous system related KEGG pathways

The 3833 and 928 unique genes derived from total proteome proteins from mouse and porcine arECMs were used to conduct a gene enrichment analysis (GEA) over GO BP, MF, CC and KEGG databases (Suppl Excel 4). The number of statistically overrepresented GO terms, after simplification, or KEGG pathways obtained in each case are summarized (Suppl. Table S6). In the total proteome scenario, results from GO CC revealed 'cell' (GO:0005623) and 'synapse' junction (GO:0045202) as the most represented hierarchies. In the matrisome-related genes subset, 'extracellular region' (GO:0005576) reached the highest proportion while 'synapse' maintained a similar percentage. Enriched GO BP and MF terms were mostly grouped into the most annotated terms described in the previous section. For both organisms, 'cellular process' (GO:0009987) and 'biological regulation' (GO:0065007) related terms were the hierarchies with the largest number of enriched terms when considering the genes derived from total proteome or the matrisome subset, respectively. Most of the enriched GO MF terms were located under the 'binding' term (GO:0005488) hierarchy.

A wide range of KEGG Pathway database subcategories was retrieved from the corresponding GEA results. In particular, 38 and 32 different subcategories were enriched from mouse and porcine arECM total proteomes, respectively (Suppl. Excel 4). For both organisms, signalling transduction, nervous and endocrine systems were the three subcategories with the largest number of overrepresented pathways.

3.7. hiPSC-derived retinal pigment epithelium cells repopulate acellular retinal ECM

Proteomic analysis showed that mouse and porcine arECMs shared a large set of proteins, despite some differences in protein levels. We hypothesized that both mouse and porcine arECM might similarly affect the integration and organization of ocular cells. To assess how ocular cells respond to arECM, we first studied the repopulation capacity of arECM as a 3D bioscaffold using a single cell type, hiPSC-derived RPE cells. We obtained a RPE cell culture that acquired pigmentation, cobblestone cell morphology, expressed bestrophin-1, MITF and ZO-1 and acquired apical-basolateral polarization (Suppl. Figure S6A), characteristic features of these cells. Then, a RPE (expressing GFP) single-cell suspension was applied onto small pieces of mouse and porcine arECM in low-attachment single wells to prevent both arECM and cells attaching to the plastic surface (Fig. 4A and B). After 48 h, remaining non-attached cells were removed and recellularized retinas allowed to proliferate for 50 days. We observed that after 12 days, RPE cells that engrafted in mouse and porcine arECMs began to compact, and at day 30, RPE started to acquire typical pigmentation, being fully pigmented at day 50 (Fig. 4C and D; Suppl. Figure S7A). By IHC of paraffin sections, we corroborated that the arECM, used as control, only contained ECM proteins (laminin and collagen I) and no DAPI staining was seen (Suppl. Figure S7B). In contrast, after 50 days of the recellularization process, we could observe that RPE-repopulated ECM were surrounded by pigmented cells (Fig. 4E; Suppl. Figure S7A) that expressed RPE specific markers such as bestrophin-1, MITF, PAX6, RPE65 and ZO-1, together with the human marker Ku80 (Fig. 4F; Suppl. Figure S7C) detected by IHC. Interestingly, in some external areas, RPE cells acquire an

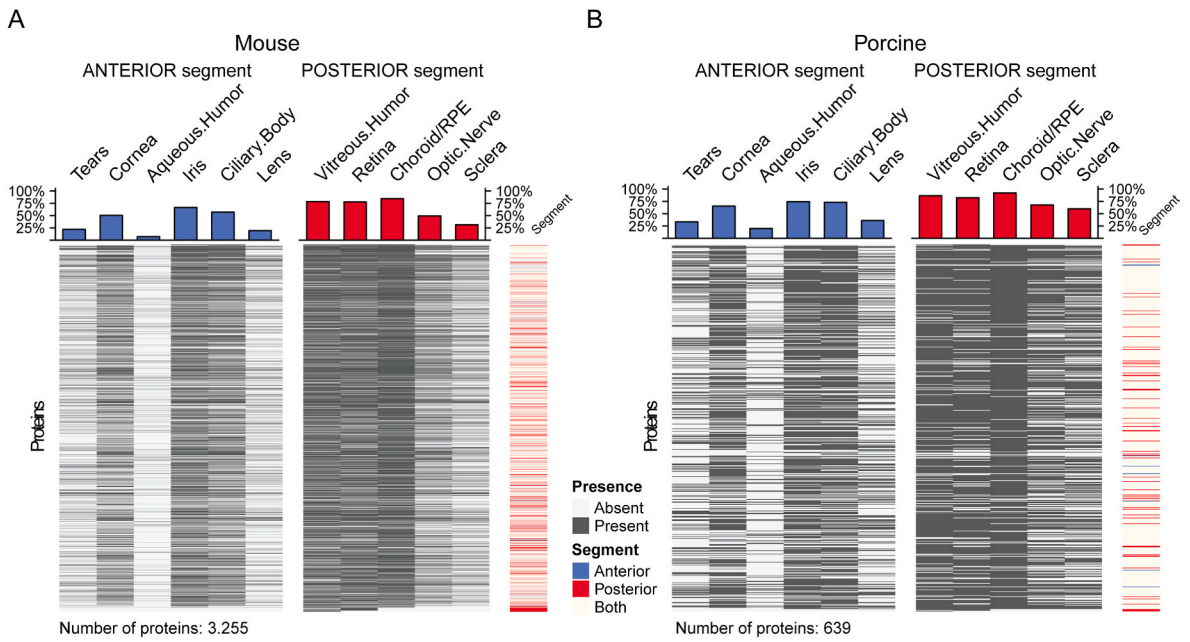

Fig. 3. Presence of mouse and porcine arECM proteins in eye tissues according to the Human EyeOme catalogue. Heatmaps show the presence/absence of the human orthologs of A) mouse (3,255) and B) pig (639) identified in our mouse and porcine proteomes and described in the Human EyeOme catalogue [45] per eye tissue. Grey-scaled heatmap columns refer to a specific eye tissue grouped in Anterior (tears, cornea, aqueous humour, iris, ciliary body and lens) and Posterior (vitreous humour, retina, choroid/RPE, optic nerve and sclera) segments. Heatmap rows refer to corresponding human orthologs. Top bar plots, blue for anterior and red for posterior segments, indicate the percentage of proteins that are present in a particular eye tissue, the retina, vitreous and the choroid/RPE being the most populated tissues in both organisms. 'Segment' column on the left in A) and B) summarizes the presence of a particular protein exclusively in Anterior (blue) or exclusively in Posterior (red) or in both segments (ivory). (For interpretation of the references to colour in this figure legend, the reader is referred to the Web version of this article.)

epithelial-like layer (Fig. 4E) with the formation of tight junctions (ZO-1) in the apical side and bestrophin-1 in the basolateral side (Fig. 4F), similar to the polarization observed in culture and in vivo. Note that RPE cells basically repopulated the surface of the ECM scaffold with little infiltration, probably due to the initial compaction of arECM. We then tested the functionality of RPE-repopulated mECM *in vitro* by analyzing its photoreceptor outer segment (POS) phagocytosis capacity compared to the RPE cells in culture. As expected, RPE cells could phagocytize FITC-labelled POS on day 30 but the RPE-repopulated mECM exhibited a 6-fold increase in internalized POS (Suppl. Figure S6B-D), suggesting that arECM enhanced RPE maturation and function.

In order to test the bio-compatibility of our GFP + RPE-repopulated mouse and porcine ECM, we performed a subcutaneous xeno-transplantation in non-immunosuppressed CD-1 mice legs. Hyperacute rejection of grafts was not observed since after 2 weeks, we could detect both transplanted GFP+/Ku80+ cells attached to the mouse muscles, accompanied by little infiltration of host Ki67+ cells but negative for CD3 and CD68 (Suppl Figure S8)

3.8. *Human ocular progenitor cells repopulated mouse and porcine acellular retinal ECM scaffolds in specific cell-type structures*

Once we confirmed that mouse and porcine arECMs were easily repopulated with RPE cells, we wondered whether the preserved structural and biochemical composition of arECM could promote the spatial organization, proliferation and differentiation of hiPSC-derived ocular progenitor cells (OPCs) in order to recapitulate the complexity of this tissue (Fig. 5A). Multi-zone OPCs were differentiated from hiPSC in 2D culture and by self-organization expanded RPE, neuroretina (NR) and surface ectoderm (SE) clusters at day 30 (Suppl. Figure S9A). Multi-zone OPCs expressed specific markers of neuroectoderm (PAX6 and SIX6), NR (CHX10, CRX, NRL, RAX and TUJ1), SE (p63, CK19), lens (γ-crystallin), stromal cells (vimentin), and RPE (MITF) detected by IHC and qPCR (Suppl. Figure S9B and S9C).

To facilitate cell migration and attachment to all scaffold surfaces, whole mouse or partial porcine arECMs were carefully placed into non-attachment wells in open conformation and the OPC single-cell suspension (at day 30 of differentiation) was applied (Fig. 5B). After 48 h, remaining non-attached cells were removed and recellularized retinas allowed to proliferate for 140 days. At 15 DIV (days *in vitro*), we first observed that pigmented cells located into a ring-like structures in the centre of the OPC-repopulated ECM (Fig. 5B and C; Suppl. Figure S10A); Suppl. Figure S11A), which were maintained over time. Form days 70 and 140, OPC-repopulated ECM expressed the eye field transcription factors *PAX6;* photoreceptor-specific *CRX*, *rhodopsin* and *recoverin*; corneal-conjunctival markers *p63, CK3, CK12*, *CK19*, *CK3, AQP1*, *COLA81*, and Na^{+}/K^{+} *-ATPase; and* RPE markers *MITF* and *PEDF,* along with a low expression of the pluripotency marker *OCT4* (Fig. 5D; Suppl. Figure S10B). The cell density and size of the OPC-repopulated ECMs increased over time, and IHC of paraffin sections revealed different structures containing well-defined cell clusters (Fig. 5C and F; Fig. 6). We observed that in the inner part of the repopulated ECM contained mainly ECM proteins (collagen I and laminin), holding pigmented cell niches that expressed typical RPE markers PAX6, MITF, RPE65 and ZO-1 (Figure 5E and 5F-a; Fig. 6A,a-c' and 6B,a-e; Suppl. Figure S10C and S11A). On the other hand, the more external parts of the OPC-repopulated ECM presented clusters of neuroretinal-like and corneal-like cells. In the most inner part, we found ganglion cells (TUJ1), Müller glia (GS) and some photoreceptors (recoverin) (Fig. 5F-c-e; Suppl. Figure S10C-D and S11 B). In this area, neurons formed synapses, as shown by synaptophysin staining (Fig. 5E–e; Suppl. Figure S10D and S11B), resembling the outer plexiform layer of native retinas. In the most outer part, astrocytes (GFAP) ran longitudinally to the layer extending their projection into the inner layer and interestingly, we observed photoreceptor cells (recoverin and opsin) in the same orientation (Fig. 5F–b; Suppl. Figure S10D and S11B).

Moreover, within OPC-repopulated ECM we also observed circular cell niches containing conjunctival epithelium cells expressing CK19,

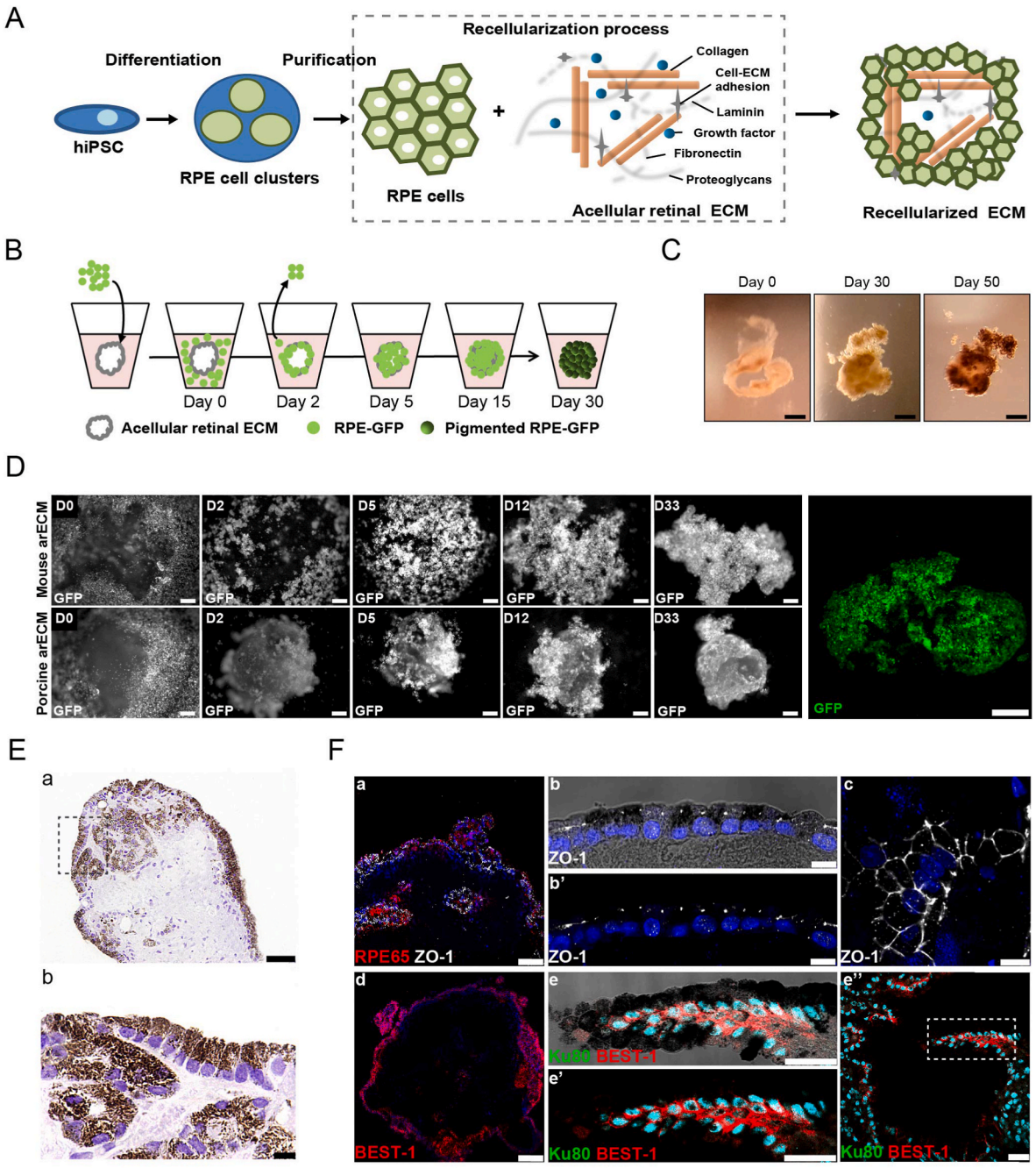

Fig. 4. hiPSC-derived RPE cells expressing GFP repopulated mouse acellular retinal ECM. A) Illustration of the RPE cell generation from hiPSC and the ECM recellularization process. B) Schematic diagram showing the arECM recellularization protocol with hiPSC-derived RPE-GFP at different time points. C) Bright field images corresponding to the arECM repopulation process. At DIV 0, acellular retinas are translucent, at DIV 30 in the recellularization process, retinas become opaque and RPE cells started to acquire pigment and at DIV 50, RPE cells are completely pigmented. Scale bars: 200 μm. D) Time lapse of GFP fluorescent images showing the recellularization of mouse arECM (top panels) or porcine arECM (bottom panels) with RPE-GFP in suspension at different time points (DIV 0, 2, 5, 12 and 33). Scale bars: 100 μm. (right) Z-stack confocal image reconstruction of recellularized mouse retina with RPE-GFP at day 35. Scale bar: 250 μm. E) Haematoxylin and eosin staining of RPE-repopulated ECM paraffin sections at DIV 50. Dashed square in (a) indicates the enlarged image in (b). Scale bars: 50 μm in a; 10 μm in b. F) Paraffin section of RPE-repopulated ECM immunolabelled with RPE-specific markers RPE65 (a), ZO-1 (a–c) and BEST-1 (d-e''). RPE cells also expressed Ku80 (human nuclear antigen; e-e''). Note that RPE cell clusters were also pigmented (bright field merged images in b and e). Interestingly, pigmented RPE cells form a polarized epithelial-like layer with tight junctions (ZO-1) in the apical site (b,b') and BEST-1 in the basolateral side (e-e''). Dashed square in (e'') indicates the area enlarged in (e and e'). Scale bar: 100 μm in d; 50 μm in a; 25 μm in e-e''; 7.5 μm in b-c. Nuclei are stained with DAPI (blue). Abbreviations: arECM, acellular retinal extracellular matrix; DIV, days *in vitro*; hiPSC, human induced pluripotent stem cells; GFP, green fluorescent protein; RPE, retinal pigment epithelium. (For interpretation of the references to colour in this figure legend, the reader is referred to the Web version of this article.)

CK5 [46], MUC1 [47] and limbal stem cell marker p63 [48] (Fig. 6A,d-f, j,k and 6B,e-g,k,n). These areas also contained keratocyte stromal cells (Vimentin) (Fig. 6A,l and 6B,m) and suprabasal cell marker Na+/K + ATPase surrounded by corneal epithelium expressing markers CK3 (Fig. 6A,g and 6B,h-i). Particular regions also exhibited the lens-specific γ-crystallin marker, as described previously [49,50] (Fig. 6A,h-i and 6B, j-l).

These results indicate that OPCs engrafted, proliferated and

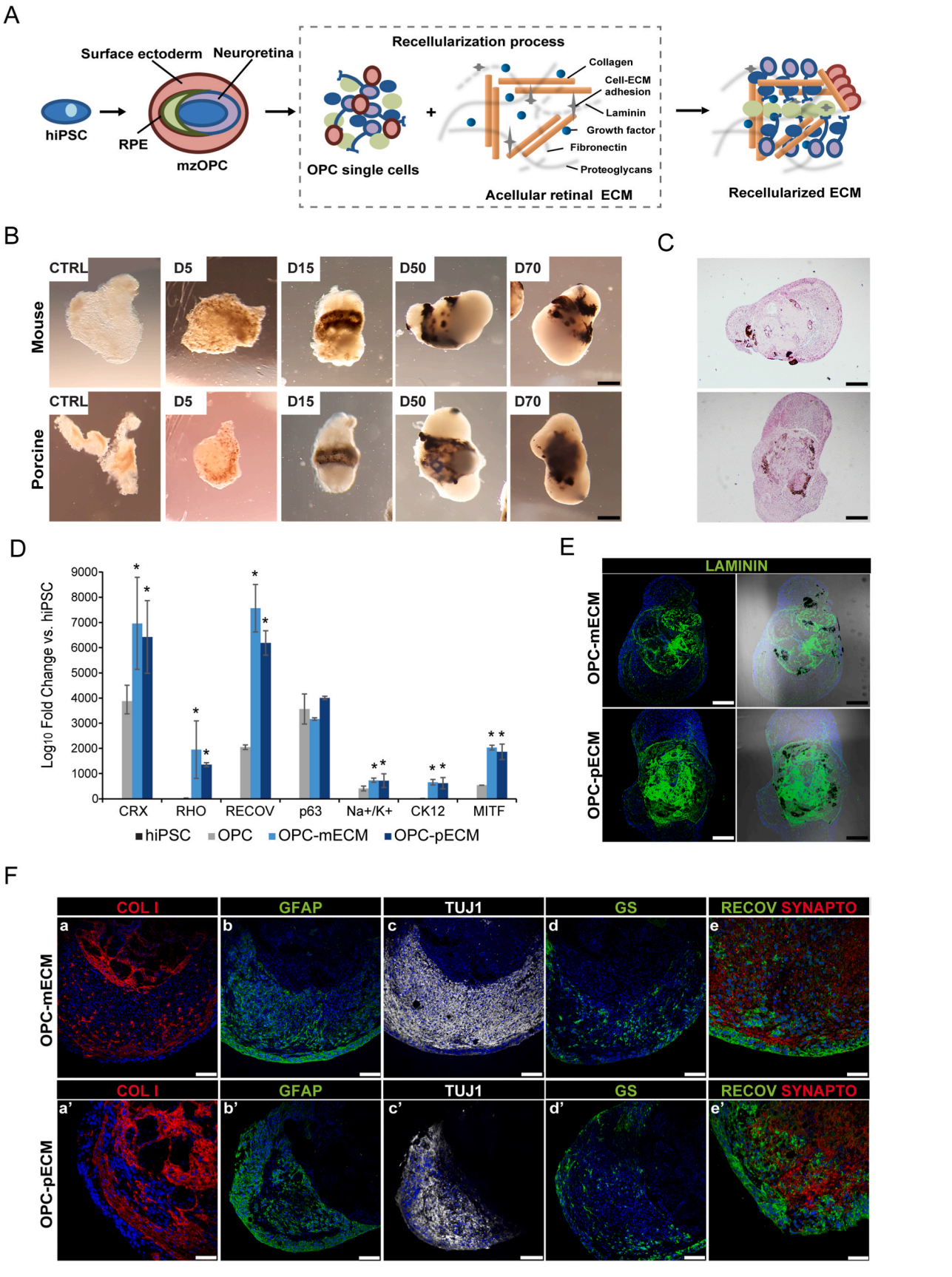

(caption on next page)

Fig. 5. OPC-repopulated mouse and porcine acellular retinal ECMs display neuro-retinal features. A) Illustration of the recellularization process of arECM with hiPSC-derived multi-zone ocular progenitor cells (mzOPC) single cells at day 30 of differentiation. OPC are composed of retinal pigment epithelium (RPE), surface ectoderm and neuroretina. B) Micrographies of the repopulation time course of mouse and porcine ECM at 5, 15, 50 and 70 DIV. Controls are arECM without cells. Scale bar: 300 μm. C) Haematoxylin and eosin staining of paraffin sections showing organization of pigmented cells. Scale bar: 200 μm. D) RT-qPCR analysis of specific photoreceptor (*CRX*, *rhodopsin* (RHO), and *recoverin* (RECOV)), conjunctival (*p63* and Na^+/K^+ *-ATPase* (Na+/K+)), corneal (*CK12*), retinal pigment epithelium (*MITF*), gene expression levels in hiPSC, OPC at 30 DIV, and OPC-repopulated mouse (OPC-mECM) and porcine (OPC-pECM) arECMs at 70 and 140 DIVs. Values are normalized to *GAPDH*. Data presented as mean ± SD (n = 3). Values indicated with stars are significantly different from those in OPC (Student's t-test; *p < 0.05). E) Bright field merged and immunostaining images of OPC-repopulated mouse and porcine ECM (OPC-mECM and OPC-pECM, respectively) labelled with ECM marker laminin. Scale bars: 250 μm. F) Confocal images of OPC-mECM and OPC-pECM labelled with neuroretinal markers glial fibrillary acidic protein (GFAP), neuron-specific class III beta-tubulin (TUJ1), presynaptic marker synaptophysin (SYNAPTO), glutamine synthetase (GS); and photoreceptor marker recoverin (RECOV). Scale bars: 100 μm (a–d), 50 μm (e). Nuclei are stained in DAPI. Abbreviations: DIV, days *in vitro*; hiPSC, human induced pluripotent stem cells; RPE, retinal pigment epithelium; OPC, ocular progenitor cells; ECM, extracellular matrix.

distributed within the mouse and the porcine arECM scaffolds in cell lineage-specific clusters. This suggests an effect of signalling molecules and structural ECM proteins retained on the arECM scaffolds on the differentiation and maturation of ocular cells.

4. Discussion

Decellularization of different tissues holds great promise in tissue engineering. Although decellularized ECM generation from bovine retina has been reported [17,18] and used as films or media supplement, its application as a 3D scaffold to host pluripotent stem cell-derived RPE or ocular progenitor cells has not been carried out previously. In this context, we hypothesized that decellularized retinas may provide the ECM with a dual role: as a supportive structure and as a storage of secreted soluble factors that might help ocular cells to engraft, proliferate, differentiate and mature as their counterparts do. Here, we presented a successful decellularization of mouse and porcine retinas while preserving their ECM structure. Using quantitative proteomic analysis, we observed that each acellular retinal ECM contains most of the ECM proteins, mainly enriched in matrisome component. But, more interestingly, 3D retinal ECM scaffolds supported RPE cell engraftment and pigmentation and OPC engraftment and maturation in cell-type- and region-type-specific clusters.

We have used a decellularization protocol that removed cellular material content from mouse and porcine retinas (94 %), similar to that reported by Kundu et al. [18], and Dorgau et al. [17], from bovine retinas. Because the retina is a soft tissue composed of a small amount of ECM, we decided to use a combination of chemical and enzymatic methods as we observed that mechanical techniques, such as freezing and thawing, destroyed the tissue structure (data not shown).

By proteomic analysis, we provided a comprehensive characterization of the arECm composition derived from mouse and porcine retinas. We found that using our decellularization protocol, mouse and porcine arECM conserved most of the common basement membrane proteins, such as collagen IV, laminins, fibronectin, tenascin, and heparan, among others [51]. Indeed, basement membranes provide a substrate for cells and release important signals for retina development. Basement membranes are composed of an inner limiting membrane (ILM) that separates the retina from the vitreous, Bruch's membrane that separates the RPE from the choroid, and vascular membrane [52–54]. Moreover, we found non-basement membrane proteins collagen type I and laminin 5, which is the interstitial matrix localized between ILM and RPE [55], together with cell adhesion proteins such as integrins, and secreted factors TGF and S100 families. We found three subcategories with more overrepresented pathways obtained in GEA analysis: signalling transduction, nervous and endocrine systems. Pathways included in the endocrine system mainly referred to signalling activity, including 'HIF-1 signalling pathway' related with retinal neuroprotection, found in both organisms, and 'VEGF signalling pathway' related with retinal vasculature. Nervous system subcategory agglutinated nine and six related pathways for mouse and porcine arECM, respectively, including ion channels and non-channel synapses such as glutamatergic, GABAergic or dopaminergic types. Interestingly, four pathways from the cellular community subcategory 'adherens junction', 'gap junction', 'tight junction' and 'focal adhesion', and 'ECM-receptor interaction' were overrepresented in both organisms. The Actin cytoskeleton reorganization path from the 'Focal adhesion' pathway was triggered by ECM molecules' (*i.e.* collagens, laminins and fibronectins) interaction mainly with integrin proteins.

To verify whether the retained complex protein composition of the acellular retinal ECM showed similarities with specific human retinal tissue, the ECM proteins quantified in our data were compared with the Human EyeOme catalogue. Currently, 9782 nonredundant proteins have been identified in the human eye [45]. We found 88–95 % of our acellular retinal ECM proteome, corresponding to human orthologs, were represented in the EyeOme, mostly associated with, but not restricted to, the retina and the RPE. Using our method, we identified a high number of ECM proteins compared with previous studies [24,56], basically because we also used UniProtKB/TrEMBL to identify porcine ECM proteins. This was a bit of a challenge as in UniProtKB/SwissProt, no porcine collagen was present.

In the last few years, recellularization of acellular organs such as cornea, lungs or heart have been postulated as promising bioengineered tissues [57,58]. In particular, decellularized retinas, Bruchs' membrane or RPE have been processed to obtain films on which retinal or RPE cells were cultured with a particular ability to enhance RPE cell and photoreceptor maturation, which suggests the retention of determinant ECM proteins and secreted factors [16–21]. However, recellularization of retinal films is currently limited by two factors: first, recellularization is generally focused on a single cell type setting aside the complexity of eye composition; and second, recellularization is usually performed in 2 dimensions, losing the 3D microenvironment composition of the native tissue matrix. To overcome these issues, we used the retinal acellular matrix as a 3D scaffold for cell repopulation purposes showing that RPE cells or OPC were able to engraft, survive, differentiate and organize within the matrix. The simplest method to repopulate the retinal ECM scaffolds is the direct application of a cell suspension of RPE cells and OPC surrounding the acellular ECM. We achieved this by culturing the cells with the arECM in suspension in low-attachment wells to prevent adhesions to the culture surface and to force cells to colonize the scaffold. Then, the repopulation of the inner parts of the scaffold relied on the cell migration capacity, as previously seen in the recellularization of corneas [59].

Pigmentation of RPE cells correlates with the differentiation status [60]. Higher pigmented RPE cells correlates with more mature and functional status. Consistently, we showed that RPE-repopulated ECM matured gradually with increasing pigment and decreasing proliferation as differentiation proceeded. Moreover, we observed that in RPE-repopulated ECM, RPE cells had limited mobility to colonize the interior part of the retinal scaffold, probably due to their maturation state [61]. In contrast, we found pigmented cell niches within the collagen and laminin matrices of both mouse and porcine OPC-repopulated ECMs. This finding suggests that pigmented cells derived from OPC cultures were still in a precursor state, which implies an increased migration capacity to populate the inner structures. The fact that we observed the same phenomenon in both species suggests

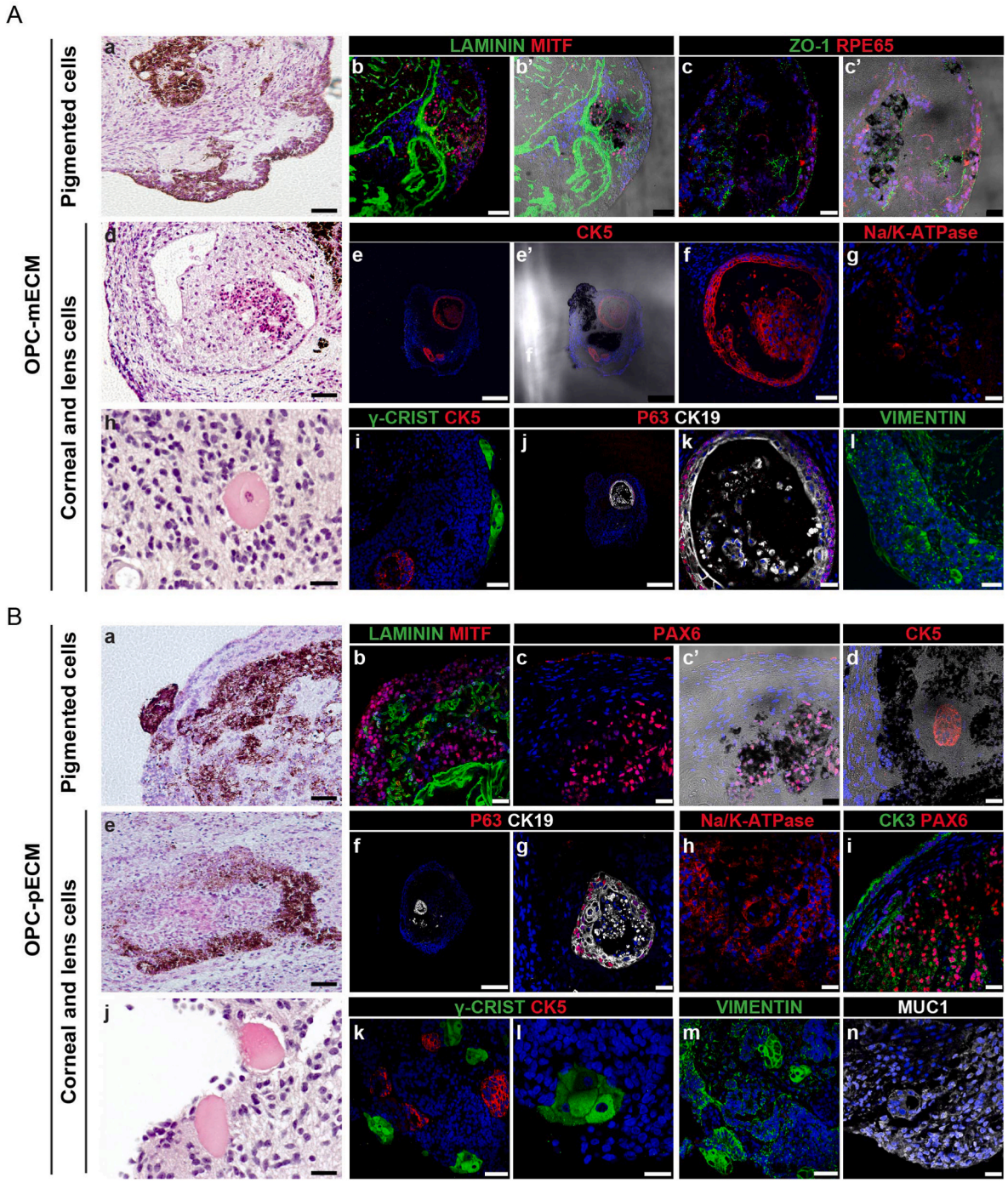

Fig. 6. OPC-repopulated mouse and porcine acellular retinal ECMs develop clusters of pigmented cells, corneal and conjunctival, stromal and lens cells. Histological and immunohistochemical analysis of (A) OPC-repopulated mouse retinal ECM (OPC-mECM) and (B) OPC-repopulated porcine retinal ECM (OPC-pECM). Paraffin sections were stained with haematoxylin and eosin (left panels) or labelled with antibodies against (right panels): ECM protein laminin; RPE markers MITF, ZO-1, PAX6 and RPE65; corneal markers cytokeratin 3 (CK3) and Na+/K + -ATPase; conjunctival markers CK19, p63 and mucin-1 (MUC1); stroma cell marker Vimentin; and lens marker γ-crystallin (γ-CRIST). Nuclei are stained with DAPI. Scale bars: A) 250 μm in e,e',j; 50 μm in a,b,b',d,f,i,l; 25 μm in c,c',g,h,k. B) 250 μm in f; 50 μm in a,d,k,m; 25 μm in b-d,g-j,l,n.

that the relative amounts and organization of particular structural proteins or secreted factors are conserved in arECMs and similarly guide these pigmented cells to migrate inside and form clusters. Additionally, in OPC-repopulated ECM where we observed pigmented cells, not all of them expressed RPE markers. The specification of RPE cells is associated with MITF expression and maturation related to MERTK, TYR, bestrophin and RPE65 and ZO-1, as we observed in the hiPSC-derived RPE [39]. The phagocytosis capacity of RPE-repopulated ECM was also assessed. Compared with RPE cells in culture, RPE cells in the repopulated ECM were highly pigmented, exhibiting increased phagocytosis of POS, which suggests that arECM enhances RPE maturation. To further assess the utility of the RPE-repopulated mouse and porcine ECM, we examined the *in vivo* biocompatibility by implanting them subcutaneously into CD-1 mice. At 2 weeks, both groups exhibited similar staining, with Ki67 proliferative cells a result of tissue injury during the implantation process and the presence of foreign material. By week 2, the

constructive cell infiltrate (CD3-/CD68-) started to degrade the grafts as we could not detect GFP + cells at 4 weeks post-transplantation. Our data suggest that the implanted repopulated ECMs last for 2 weeks with a low inflammatory response, which may be improved by the immunosuppression of the animals.

By using hiPSC-derived OPC, which contain progenitors of different ocular cells, we mimicked the complex cellular composition of the eye, as we observed areas of repopulated ECM containing clusters of retinal cells, pigmented cells, corneal-like cells, stroma cells and lens. In previous studies, retinal organoids originated from hiPSC cultures presented lamination of the retina with photoreceptor layer, bipolar progenitors and ganglion cells resembling retinal structure [62]. Here, repopulation of arECM with multi-zone OPC did not yield the same retinal organization observed in retinal organoids or native retinas, probably because of the disaggregation of 2D retinal structures before the repopulation and the effect of ECM structural proteins and biological cues on OPC organization. The interactions between ECMs and cell receptors can directly influence the intracellular signal pathways. Despite that, OPC integrated and maturated within the ECM, and showed a certain degree of cell-specific organization mainly composed of photoreceptors, ganglion cells, astrocytes (GFAP marker) and Müller glia (glutamine synthetase), these glial cells being difficult to develop in retinal organoids [63]. These differences may be attributed to ECM extrinsic cues involved in retinal cell fate determination, such as laminins, whose expression is spatially and temporally associated with retinal development [64]. On the other hand, multi-zone OPC gave rise to translucent corneal organoids with stroma cells and Bowman's-like membrane [65]. Here, repopulated ECM with OPC also supported anterior segment of the eye proteins such as conjunctival, corneal and lens cells, which organized in a cluster, although not comparable to the organization of native corneas. We did not observe any translucent structure resembling corneal organoids probably due to the engraftment of these cells inside the compact ECM. The organization and maturation of corneal-like cells could have been possible as arECM also contained protein present in the anterior segment of the eye.

Our current study has several limitations. A partial ECM insoluble fraction could be lost in our samples. The high insolubility of ECM proteins represents a challenge in proteomic analysis, and a complete solubilisation requires conditions incompatible with mass spectrometry [66]. The differences among the most abundant proteins between mouse and pig may be attributed to (i) the manual retinas isolation process, (ii) different phenotype traits between organisms that affect the proteome, (iii) use of a non-curated protein database for pig and (iv) arbitrary selection criteria. Furthermore, repopulated retinas failed to maintain their structure and conformation, likely due to the softness of the ECM and the cell-cell interaction of engrafted cells that forced repopulated-ECM to fold. Therefore, repopulation of the ECM did not yield the native retinal cell organization. Effective retinal organization in acellular retinal ECM is biologically complicated and requires the delivery and distribution of progenitor cells, integration and organization of those cells into the retinal layers, differentiation into the mature cell type, and formation of correct synaptic connections. All these, together with their big size and 3D conformation, hinder the application of our repopulated-ECM for therapeutic purposes. Therefore, future cell repopulation studies using novel ECM-derived hydrogels or films may further help to conserve the retinal morphology and may be more optimal for retinal regenerative purposes.

5. Conclusion

To date, no studies are available on the recellularization properties of the entire acellular retina used as a 3D scaffold. In this study, we show that repopulation of murine and porcine retinal decellularized matrices, either with hiPSC-derived RPE cells or ocular precursor cells, led to cellular proliferation and maturation within the matrix in cell-specific clusters, indicating that acellular retinal ECM may retain native components that guide cell adhesion, migration and organization. Moreover, proteomic analysis of decellularized retinas may allow the identification of novel ECM matrix components, receptors and soluble factors or active molecules which may be important to improve cell-based therapies to treat retinal diseases, as well as to develop biocompatible artificial scaffolds that improve cell survival and to promote retinal regeneration. These results provide insight into the microenvironment niche through decellularization of native retinal ECM that preserves its complex functional and structural proteins of glycosaminoglycans (GAGs), glycoproteins, and bioactive cues. It is difficult, however, to accurately mimic native ECM beyond the capacity of synthetic engineering.

Funding

This work was supported by La Marató de TV3 Foundation (484/C/2012); ERA-NET EuroNanoMed III-AC19/00080/ISCIII (CELLUX); Instituto de Salud Carlos III (CA18/00045 and PI18/00219); and the European Social Fund, the Ministerio de Ciencia, Innovación y Universidades, which is part of the Agencia Estatal de Investigación (PTA2018-016371-I). A.D. was supported by PT13/0001/0041 PRB2-ISCIII-SGEFI-FEDER-PE I+D+i 2013–2016 and ISCIII-FEDER RETICS (Oftared; RD16/0008). We thank the CERCA Programme/Generalitat de Catalunya for institutional support.

Data availability

The raw data and the processed data required to reproduce these findings are available in the Supplementary Excels.

Author contributions

Maria Maqueda: Conceptualization, Methodology, Software, Formal analysis, Resources, Data curation, Writing – original draft, Visualization. Jose Luis Mosquera: Conceptualization, Methodology, Software, Formal analysis, Resources, Data curation, Writing – original draft, Visualization. José García-Arumí: Writing – review & editing, Funding acquisition. Anna Veiga: Writing – review & editing, Funding acquisition. Anna Duarri: Conceptualization, Methodology, Validation, Investigation, Writing – original draft, Writing – review & editing, Visualization, Supervision, Funding acquisition.

Declaration of competing interest

The authors declare that they have no known competing financial interests or personal relationships that could have appeared to influence the work reported in this paper.

Acknowledgments

We thank Lola Mulero, Begoña Aran, Bernd Kuebler and Joan Josep Bech for technical assistance. Histological processing was performed by the Histology Unit at IDIBELL, and by the ICTS-NANBIOSIS-U20/FVPR at the Vall d'Hebron Institute of Research. LC-MS/MS was conducted by Clinical Proteomics Unit, Bellvitge Biomedical Research Institute (IDIBELL).

Appendix A. Supplementary data

Supplementary data to this article can be found online at https://doi.org/10.1016/j.biomaterials.2021.121049.

References

[1] E.A. Bassett, V.A. Wallace, Cell fate determination in the vertebrate retina, Trends Neurosci. 35 (2012) 565–573, https://doi.org/10.1016/j.tins.2012.05.004.

[2] Y. Lu, W. Yi, Q. Wu, S. Zhong, Z. Zuo, F. Zhao, M. Zhang, N. Tsai, Y. Zhuo, S. He, J. Zhang, X. Duan, X. Wang, T. Xue, Single-cell RNA-seq analysis maps the development of human fetal retina, BioRxiv (2018) 423830, https://doi.org/10.1101/423830.

[3] L. Hackler, J. Wan, A. Swaroop, J. Qian, D.J. Zack, MicroRNA profile of the developing mouse retina, Invest. Ophthalmol. Vis. Sci. 51 (2010) 1823–1831, https://doi.org/10.1167/iovs.09-4657.

[4] M. Felemban, B. Dorgau, N.C. Hunt, D. Hallam, D. Zerti, R. Bauer, Y. Ding, J. Collin, D. Steel, N. Krasnogor, J. Al-Aama, S. Lindsay, C. Mellough, M. Lako, Extracellular matrix component expression in human pluripotent stem cell-derived retinal organoids recapitulates retinogenesis in vivo and reveals an important role for IMPG1 and CD44 in the development of photoreceptors and interphotoreceptor matrix, Acta Biomater. 74 (2018) 207–221, https://doi.org/10.1016/j.actbio.2018.05.023.

[5] M.I. Willardsen, B.A. Link, Cell biological regulation of division fate in vertebrate neuroepithelial cells, Dev. Dyn. Off. Publ. Am. Assoc. Anat. 240 (2011) 1865–1879, https://doi.org/10.1002/dvdy.22684.

[6] R.E. Hausman, Ocular extracellular matrices in development, Prog. Retin. Eye Res. 26 (2007) 162–188, https://doi.org/10.1016/j.preteyeres.2006.11.001.

[7] R.T. Libby, W.J. Brunken, D.D. Hunter, Roles of the extracellular matrix in retinal development and maintenance, Results Probl. Cell Differ. 31 (2000) 115–140.

[8] S. Aisenbrey, M. Zhang, D. Bacher, J. Yee, W.J. Brunken, D.D. Hunter, Retinal pigment epithelial cells synthesize laminins, including laminin 5, and adhere to them through α3- and α6-containing integrins, Invest. Ophthalmol. Vis. Sci. 47 (2006) 5537–5544, https://doi.org/10.1167/iovs.05-1590.

[9] A.M. Kolomeyer, I.K. Sugino, M.A. Zarbin, Characterization of conditioned media collected from cultured adult versus fetal retinal pigment epithelial cells, Invest. Ophthalmol. Vis. Sci. 52 (2011) 5973–5986, https://doi.org/10.1167/iovs.10-6965.

[10] J.C. Booij, D.C. Baas, J. Beisekeeva, T.G.M.F. Gorgels, A.a.B. Bergen, The dynamic nature of Bruch's membrane, Prog. Retin. Eye Res. 29 (2010) 1–18, https://doi.org/10.1016/j.preteyeres.2009.08.003.

[11] S.J. Clark, T.D.L. Keenan, H.L. Fielder, L.J. Collinson, R.J. Holley, C.L.R. Merry, T. H. van Kuppevelt, A.J. Day, P.N. Bishop, Mapping the differential distribution of glycosaminoglycans in the adult human retina, choroid, and sclera, Invest. Ophthalmol. Vis. Sci. 52 (2011) 6511–6521, https://doi.org/10.1167/iovs.11-7909.

[12] T.D.L. Keenan, S.J. Clark, R.D. Unwin, L.A. Ridge, A.J. Day, P.N. Bishop, Mapping the differential distribution of proteoglycan core proteins in the adult human retina, choroid, and sclera, Invest. Ophthalmol. Vis. Sci. 53 (2012) 7528–7538, https://doi.org/10.1167/iovs.12-10797.

[13] R.O. Hynes, A. Naba, Overview of the matrisome—an inventory of extracellular matrix constituents and functions, Cold Spring Harb. Perspect. Biol. (2011) a004903, https://doi.org/10.1101/cshperspect.a004903.

[14] A. Naba, K.R. Clauser, S. Hoersch, H. Liu, S.A. Carr, R.O. Hynes, The matrisome: in silico definition and in vivo characterization by proteomics of normal and tumor extracellular matrices, Mol. Cell. Proteomics (2011), https://doi.org/10.1074/mcp.M111.014647.

[15] A. Porzionato, E. Stocco, S. Barbon, F. Grandi, V. Macchi, R. De Caro, Tissue-engineered grafts from human decellularized extracellular matrices: a systematic review and future perspectives, Int. J. Mol. Sci. 19 (2018), https://doi.org/10.3390/ijms19124117.

[16] K.R. Chirco, K.S. Worthington, M.J. Flamme-Wiese, M.J. Riker, J.D. Andrade, B. M. Ueberheide, E.M. Stone, B.A. Tucker, R.F. Mullins, Preparation and evaluation of human choroid extracellular matrix scaffolds for the study of cell replacement strategies, Acta Biomater. 57 (2017) 293–303, https://doi.org/10.1016/j.actbio.2017.05.011.

[17] B. Dorgau, M. Felemban, G. Hilgen, M. Kiening, D. Zerti, N.C. Hunt, M. Doherty, P. Whitfield, D. Hallam, K. White, Y. Ding, N. Krasnogor, J. Al-Aama, H.Z. Asfour, E. Sernagor, M. Lako, Decellularised extracellular matrix-derived peptides from neural retina and retinal pigment epithelium enhance the expression of synaptic markers and light responsiveness of human pluripotent stem cell derived retinal organoids, Biomaterials 199 (2019) 63–75, https://doi.org/10.1016/j.biomaterials.2019.01.028.

[18] J. Kundu, A. Michaelson, K. Talbot, P. Baranov, M.J. Young, R.L. Carrier, Decellularized retinal matrix: natural platforms for human retinal progenitor cell culture, Acta Biomater. 31 (2016) 61–70, https://doi.org/10.1016/j.actbio.2015.11.028.

[19] S. McLenachan, E. Hao, D. Zhang, L. Zhang, M. Edel, F. Chen, Bioengineered Bruch's-like extracellular matrix promotes retinal pigment epithelial differentiation, Biochem. Biophys. Rep. 10 (2017) 178–185, https://doi.org/10.1016/j.bbrep.2017.03.008.

[20] S. Ponce Márquez, V.S. Martínez, W. McIntosh Ambrose, J. Wang, N.G. Gantxegui, O. Schein, J. Elisseeff, Decellularization of bovine corneas for tissue engineering applications, Acta Biomater. 5 (2009) 1839–1847, https://doi.org/10.1016/j.actbio.2009.02.011.

[21] T.H. Tezel, L.V.D. Priore, H.J. Kaplan, Reengineering of aged Bruch's membrane to enhance retinal pigment epithelium repopulation, Invest. Ophthalmol. Vis. Sci. 45 (2004) 3337–3348, https://doi.org/10.1167/iovs.04-0193.

[22] J. Cox, M. Mann, MaxQuant enables high peptide identification rates, individualized p.p.b.-range mass accuracies and proteome-wide protein quantification, Nat. Biotechnol. 26 (2008) 1367–1372, https://doi.org/10.1038/nbt.1511.

[23] J. Cox, N. Neuhauser, A. Michalski, R.A. Scheltema, J.V. Olsen, M. Mann, Andromeda: a peptide search engine integrated into the MaxQuant environment, J. Proteome Res. 10 (2011) 1794–1805, https://doi.org/10.1021/pr101065j.

[24] UniProt Consortium, UniProt: a worldwide hub of protein knowledge, Nucleic Acids Res. 47 (2019) D506–D515, https://doi.org/10.1093/nar/gky1049.

[25] R.C. Gentleman, V.J. Carey, D.M. Bates, B. Bolstad, M. Dettling, S. Dudoit, B. Ellis, L. Gautier, Y. Ge, J. Gentry, K. Hornik, T. Hothorn, W. Huber, S. Iacus, R. Irizarry, F. Leisch, C. Li, M. Maechler, A.J. Rossini, G. Sawitzki, C. Smith, G. Smyth, L. Tierney, J.Y.H. Yang, J. Zhang, Bioconductor: open software development for computational biology and bioinformatics, Genome Biol. 5 (2004) R80, https://doi.org/10.1186/gb-2004-5-10-r80.

[26] org.Mm.eg M. Carlson, Db: Genome Wide Annotation for Mouse. R Package, version 3.8.2, 2019.

[27] org.Ss.eg M. Carlson, Db: Genome Wide Annotation for Pig. R Package, version 3.8.2, 2019.

[28] S. Durinck, Y. Moreau, A. Kasprzyk, S. Davis, B. De Moor, A. Brazma, W. Huber, BioMart and Bioconductor: a powerful link between biological databases and microarray data analysis, Bioinformatics 21 (2005) 3439–3440, https://doi.org/10.1093/bioinformatics/bti525.

[29] W. Huber, V.J. Carey, R. Gentleman, S. Anders, M. Carlson, B.S. Carvalho, H. C. Bravo, S. Davis, L. Gatto, T. Girke, R. Gottardo, F. Hahne, K.D. Hansen, R. A. Irizarry, M. Lawrence, M.I. Love, J. MacDonald, V. Obenchain, A.K. Oleś, H. Pagès, A. Reyes, P. Shannon, G.K. Smyth, D. Tenenbaum, L. Waldron, M. Morgan, Orchestrating high-throughput genomic analysis with Bioconductor, Nat. Methods 12 (2015) 115–121, https://doi.org/10.1038/nmeth.3252.

[30] Ensembl D.R. Zerbino, P. Achuthan, W. Akanni, M.R. Amode, D. Barrell, J. Bhai, K. Billis, C. Cummins, A. Gall, C.G. Girón, L. Gil, L. Gordon, L. Haggerty, E. Haskell, T. Hourlier, O.G. Izuogu, S.H. Janacek, T. Juettemann, J.K. To, M.R. Laird, I. Lavidas, Z. Liu, J.E. Loveland, T. Maurel, W. McLaren, B. Moore, J. Mudge, D. N. Murphy, V. Newman, M. Nuhn, D. Ogeh, C.K. Ong, A. Parker, M. Patricio, H. S. Riat, H. Schuilenburg, D. Sheppard, H. Sparrow, K. Taylor, A. Thormann, A. Vullo, B. Walts, A. Zadissa, A. Frankish, S.E. Hunt, M. Kostadima, N. Langridge, F.J. Martin, M. Muffato, E. Perry, M. Ruffier, D.M. Staines, S.J. Trevanion, B. L. Aken, F. Cunningham, A. Yates, P. Flicek, 2018, Nucleic Acids Res. 46 (2018) D754–D761, https://doi.org/10.1093/nar/gkx1098.

[31] M. Ashburner, C.A. Ball, J.A. Blake, D. Botstein, H. Butler, J.M. Cherry, A.P. Davis, K. Dolinski, S.S. Dwight, J.T. Eppig, M.A. Harris, D.P. Hill, L. Issel-Tarver, A. Kasarskis, S. Lewis, J.C. Matese, J.E. Richardson, M. Ringwald, G.M. Rubin, G. Sherlock, Gene Ontology: tool for the unification of biology, Nat. Genet. 25 (2000) 25–29, https://doi.org/10.1038/75556.

[32] M. Carlson, G.O. db, A set of annotation maps describing the entire Gene Ontology. R Package, 2019, version 3.8.2.

[33] H. Wickham, ggplot2: Elegant Graphics for Data Analysis, Springer-Verlag, New York, 2016.

[34] M. Kanehisa, S. Goto, KEGG: Kyoto Encyclopedia of genes and Genomes, Nucleic Acids Res. 28 (2000) 27–30, https://doi.org/10.1093/nar/28.1.27.

[35] G. Yu, L.-G. Wang, Y. Han, Q.-Y. He, clusterProfiler: an R Package for comparing biological themes among gene clusters, OMICS A J. Integr. Biol. 16 (2012) 284–287, https://doi.org/10.1089/omi.2011.0118.

[36] Y. Benjamini, Y. Hochberg, Controlling the False discovery rate: a practical and powerful approach to multiple testing, J. R. Stat. Soc. Ser. B Methodol. 57 (1995) 289–300, https://doi.org/10.1111/j.2517-6161.1995.tb02031.x.

[37] L. Miquel-Serra, A. Duarri, Y. Muñoz, B. Kuebler, B. Aran, C. Costa, M. Martí, M. Comabella, S. Malhotra, X. Montalban, A. Veiga, A. Raya, Generation of six multiple sclerosis patient-derived induced pluripotent stem cell lines, Stem Cell Res. 24 (2017) 155–159, https://doi.org/10.1016/j.scr.2017.06.001.

[38] R. Hayashi, Y. Ishikawa, R. Katori, Y. Sasamoto, Y. Taniwaki, H. Takayanagi, M. Tsujikawa, K. Sekiguchi, A.J. Quantock, K. Nishida, Coordinated generation of multiple ocular-like cell lineages and fabrication of functional corneal epithelial cell sheets from human iPS cells, Nat. Protoc. 12 (2017) 683–696, https://doi.org/10.1038/nprot.2017.007.

[39] M. Riera, L. Fontrodona, S. Albert, D.M. Ramirez, A. Seriola, A. Salas, Y. Muñoz, D. Ramos, M.P. Villegas-Perez, M.A. Zapata, A. Raya, J. Ruberte, A. Veiga, J. Garcia-Arumi, Comparative study of human embryonic stem cells (hESC) and human induced pluripotent stem cells (hiPSC) as a treatment for retinal dystrophies, Mol. Ther. Methods Clin. Dev. 3 (2016) 16010, https://doi.org/10.1038/mtm.2016.10.

[40] A. Salas, A. Duarri, L. Fontrodona, D.M. Ramírez, A. Badia, H. Isla-Magrané, B. Ferreira-de-Souza, M.Á. Zapata, Á. Raya, A. Veiga, J. García-Arumí, Cell therapy with human induced pluripotent stem cell-derived retinal pigment epithelium and retinal precursor cells prevents visual function loss in a rat model of retinal degeneration, Mol. Ther. - Methods Clin. Dev. (2021), https://doi.org/10.1016/j.omtm.2021.02.006.

[41] A. Badia, A. Salas, A. Duarri, B. Ferreira-de-Souza, M.Á. Zapata, L. Fontrodona, J. García-Arumí, Transcriptomics analysis of Ccl2/Cx3cr1/Crb1rd8 deficient mice provides new insights into the pathophysiology of progressive retinal degeneration, Exp. Eye Res. 203 (2021) 108424, https://doi.org/10.1016/j.exer.2020.108424.

[42] E. Vecino, J.P. Heller, P. Veiga-Crespo, K.R. Martin, J.W. Fawcett, Influence of extracellular matrix components on the expression of integrins and regeneration of adult retinal ganglion cells, PloS One 10 (2015), e0125250, https://doi.org/10.1371/journal.pone.0125250.

[43] H. Ragelle, A. Naba, B.L. Larson, F. Zhou, M. Prijić, C.A. Whittaker, A. Del Rosario, R. Langer, R.O. Hynes, D.G. Anderson, Comprehensive proteomic characterization of stem cell-derived extracellular matrices, Biomaterials 128 (2017) 147–159, https://doi.org/10.1016/j.biomaterials.2017.03.008.

[44] J.C. Harman, J.J. Guidry, J.M. Gidday, Comprehensive characterization of the adult ND4 Swiss Webster mouse retina: using discovery-based mass spectrometry to decipher the total proteome and phosphoproteome, Mol. Vis. 24 (2018) 875–889.

[45] M.T. Ahmad, P. Zhang, C. Dufresne, L. Ferrucci, R.D. Semba, The human eye proteome Project: updates on an emerging proteome, Proteomics 18 (2018) 1700394, https://doi.org/10.1002/pmic.201700394.
[46] S. Merjava, A. Neuwirth, M. Tanzerova, K. Jirsova, The spectrum of cytokeratins expressed in the adult human cornea, limbus and perilimbal conjunctiva, Histol. Histopathol. 26 (2011) 323–331, https://doi.org/10.14670/HH-26.323.
[47] V. Barbaro**, S. Ferrari**, M. Parekh, D. Ponzin, C. Parolin, E.D. Iorio, Laser scanning confocal microscopy: application in manufacturing and Research of corneal stem cells, confocal laser microsc. - princ, Appl. Med. Biol. Food Sci. (2013), https://doi.org/10.5772/55809.
[48] Z. Chen, C.S. de Paiva, L. Luo, F.L. Kretzer, S.C. Pflugfelder, D.-Q. Li, Characterization of putative stem cell phenotype in human limbal epithelia, Stem Cells Dayt. Ohio. 22 (2004) 355–366, https://doi.org/10.1634/stemcells.22-3-355.
[49] Q. Fu, Z. Qin, X. Jin, L. Zhang, Z. Chen, J. He, J. Ji, K. Yao, Generation of functional lentoid bodies from human induced pluripotent stem cells derived from urinary cells, Invest. Ophthalmol. Vis. Sci. 58 (2017) 517–527, https://doi.org/10.1167/iovs.16-20504.
[50] C. Yang, Y. Yang, L. Brennan, E.E. Bouhassira, M. Kantorow, A. Cvekl, Efficient generation of lens progenitor cells and lentoid bodies from human embryonic stem cells in chemically defined conditions, FASEB J 24 (2010) 3274–3283, https://doi.org/10.1096/fj.10-157255.
[51] D. Hubmacher, S.S. Apte, The biology of the extracellular matrix: novel insights, Curr. Opin. Rheumatol. 25 (2013) 65–70, https://doi.org/10.1097/BOR.0b013e32835b137b.
[52] M. Balasubramani, E.M. Schreiber, J. Candiello, G.K. Balasubramani, J. Kurtz, W. Halfter, Molecular interactions in the retinal basement membrane system: a proteomic approach, Matrix Biol. 29 (2010) 471–483, https://doi.org/10.1016/j.matbio.2010.04.002.
[53] J.A. Jerdan, B.M. Glaser, Retinal microvessel extracellular matrix: an immunofluorescent study, Invest. Ophthalmol. Vis. Sci. 27 (1986) 194–203.
[54] G. Uechi, Z. Sun, E.M. Schreiber, W. Halfter, M. Balasubramani, Proteomic view of basement membranes from human retinal blood vessels, inner limiting membranes, and lens capsules, J. Proteome Res. 13 (2014) 3693–3705, https://doi.org/10.1021/pr5002065.
[55] L. Taylor, K. Arnér, K. Engelsberg, F. Ghosh, Scaffolding the retina: the interstitial extracellular matrix during rat retinal development, Int. J. Dev. Neurosci. Off. J. Int. Soc. Dev. Neurosci. 42 (2015) 46–58, https://doi.org/10.1016/j.ijdevneu.2015.03.002.
[56] C. Schmelter, S. Funke, J. Treml, A. Beschnitt, N. Perumal, C. Manicam, N. Pfeiffer, F.H. Grus, Comparison of two solid-phase extraction (SPE) methods for the identification and quantification of porcine retinal protein markers by LC-MS/MS, Int. J. Mol. Sci. 19 (2018) 3847, https://doi.org/10.3390/ijms19123847.
[57] J. Fernández-Pérez, M. Ahearne, Decellularization and recellularization of cornea: progress towards a donor alternative, Methods San Diego Calif (2019), https://doi.org/10.1016/j.ymeth.2019.05.009.
[58] P.T. Moser, H.C. Ott, Recellularization of organs: what is the future for solid organ transplantation? Curr. Opin. Organ Transplant. 19 (2014) 603–609, https://doi.org/10.1097/MOT.0000000000000131.
[59] M. Gonzalez-Andrades, J.D.L.C. Cardona, A.M. Ionescu, A. Campos, M. del M. Perez, M. Alaminos, Generation of bioengineered corneas with decellularized xenografts and human keratocytes, Invest. Ophthalmol. Vis. Sci. 52 (2011) 215–222, https://doi.org/10.1167/iovs.09-4773.
[60] S.D. Schwartz, J.-P. Hubschman, G. Heilwell, V. Franco-Cardenas, C.K. Pan, R. M. Ostrick, E. Mickunas, R. Gay, I. Klimanskaya, R. Lanza, Embryonic stem cell trials for macular degeneration: a preliminary report, Lancet 379 (2012) 713–720, https://doi.org/10.1016/S0140-6736(12)60028-2.
[61] R.J. Davis, N.M. Alam, C. Zhao, C. Müller, J.S. Saini, T.A. Blenkinsop, F. Mazzoni, M. Campbell, S.M. Borden, C.J. Charniga, P.L. Lederman, V. Aguilar, M. Naimark, M. Fiske, N. Boles, S. Temple, S.C. Finnemann, G.T. Prusky, J.H. Stern, The developmental stage of adult human stem cell-derived retinal pigment epithelium cells influences transplant efficacy for vision rescue, Stem Cell Rep 9 (2017) 42–49, https://doi.org/10.1016/j.stemcr.2017.05.016.
[62] E.E. Capowski, K. Samimi, S.J. Mayerl, M.J. Phillips, I. Pinilla, S.E. Howden, J. Saha, A.D. Jansen, K.L. Edwards, L.D. Jager, K. Barlow, R. Valiauga, Z. Erlichman, A. Hagstrom, D. Sinha, V.M. Sluch, X. Chamling, D.J. Zack, M. C. Skala, D.M. Gamm, Reproducibility and Staging of 3D Human Retinal Organoids across Multiple Pluripotent Stem Cell Lines, vol. 146, Development, 2019, https://doi.org/10.1242/dev.171686.
[63] S.H. Chung, W. Shen, K.C. Davidson, A. Pébay, R.C.B. Wong, B. Yau, M. Gillies, Differentiation of retinal glial cells from human embryonic stem cells by promoting the notch signaling pathway, Front. Cell. Neurosci. 13 (2019), https://doi.org/10.3389/fncel.2019.00527.
[64] B. Dorgau, M. Felemban, A. Sharpe, R. Bauer, D. Hallam, D.H. Steel, S. Lindsay, C. Mellough, M. Lako, Laminin γ3 plays an important role in retinal lamination, photoreceptor organisation and ganglion cell differentiation, Cell Death Dis. 9 (2018), https://doi.org/10.1038/s41419-018-0648-0.
[65] P.J. Susaimanickam, S. Maddileti, V.K. Pulimamidi, S.R. Boyinpally, R.R. Naik, M. N. Naik, G.B. Reddy, V.S. Sangwan, I. Mariappan, Generating minicorneal organoids from human induced pluripotent stem cells, Dev. Camb. Engl. 144 (2017) 2338–2351, https://doi.org/10.1242/dev.143040.
[66] A. Naba, K.R. Clauser, H. Ding, C.A. Whittaker, S.A. Carr, R.O. Hynes, The extracellular matrix: tools and insights for the "omics" era, Matrix Biol. 49 (2016) 10–24, https://doi.org/10.1016/j.matbio.2015.06.003.